FACULDADE DE ENGENHARIA DA UNIVERSIDADE DO PORTO

Heat Treatment of a AISI H11 Premium Hot-Work Tool Steel

Isabel Maria Martins Miranda

Mestrado em Engenharia de Materiais

Supervisor: Profª Dr.ª Laura Ribeiro

September 17, 2024

Heat Treatment of a AISI H11 Premium Hot-Work Tool Steel

Isabel Maria Martins Miranda

Mestrado em Engenharia de Materiais

Approved in oral examination by the committee:

Candidate: Isabel Maria Martins Miranda
Code: 201907957
Title: Heat Treatment of a AISI H11 Premium Hot-Work Tool Steel
Date: September 17, 2024
Location: Faculty of Engineering of University of Porto - Room F106 - 10:00h
Chair: Prof. Dr.ª Sónia Simões
External Examiner: Prof. Dr.ª Teresa Duarte
Supervisor: Prof. Dr.ª Laura Ribeiro

September 17, 2024

Abstract

This study examines the optimisation of heat treatment parameters for AISI H11 Premium, a hot work tool steel, with the objective of enhancing its performance in demanding applications. The study emphasises the necessity of precise control of the austenitisation, quenching and tempering processes in order to achieve the desired mechanical properties while minimising production time and cost. It is well established that when heat treatment is conducted, particularly in the case of austenitisation of large components, a thermal gradient is to be expected. This is due to the fact that the centre of the tool heats at a slower rate, which results in this region reaching the desired temperature at a later point in time. Upon entering the austenitisation stage, the surface of the tool experiences a longer holding time than the centre. Should austenitisation or tempering commence at a temperature that is a few degrees Celsius below the desired temperature, it is possible to achieve considerable savings in the total time required to heat treat the component, provided that the desired microstructure uniformity and hardness are not compromised. A series of experimental procedures, including microstructural and mechanical characterisation, were employed to evaluate a range of heat treatment cycles with shorter cycles on the material in question. The heat treatment cycles were selected based on the heating rate of the surface and that of the centre, as well as on the typical holding time required for this type of steel. In light of the aforementioned considerations, the typical holding time was established as a baseline, upon which shorter holding times were selected based on the temperature at which the timer for the stage is initiated. The optimal results for quenching were achieved when a ΔT of 20°C was applied, resulting in a martensitic microstructure with minimal undissolved carbides and a hardness of 53 HRC $\pm$ 1 HRC for the centre and 46 HRC $\pm$ 1 HRC for the surface of the tool, with retained austenite below 5 %. The application of triple tempering starting 20 ºC below 560 ºC, resulted in the formation of a tempered martensitic matrix characterised by a notable dispersion of carbides, including Fe. Mo and Cr rich carbides. This heat treatment modification also yielded a hardness of 50 HRC $\pm$ 1 HRC and an impact strength of 9 J $\pm$ 3 J, properties related to the centre of the tool. In contrast, a hardness of 44 HRC $\pm$ 1 HRC and an impact strength of 15 J $\pm$ 1 J were observed for the surface of the tool. The results demonstrate the impact of varying heat treatment conditions on the hardness, grain size and carbide distribution of the steel. The findings offer valuable insights into the optimisation of the heat treatment process of the AISI H11 Premium steel, contributing to enhanced tool longevity and performance in industrial applications.

Keywords: AISI H11 Premium, Carbide Precipitation, Improvement, Quenching, Rockwell-C Hardness, Scanning Electron Microscopy (SEM)/Energy-Dispersive X-ray Spectroscopy (EDS), Tempering, Toughness.

Resumo

Este estudo compreende a otimização dos parâmetros de tratamento térmico do um aço ferramenta para trabalho a quente AISI H11 Premium, com o objetivo de melhorar o seu desempenho em situações críticas. Este estudo salienta a necessidade de um controlo rigoroso dos processos de austenitização, têmpera e revenido, a fim de obter as propriedades mecânicas desejadas, minimizando o tempo e o custo do processo. É estabelecido que, sobretudo no caso da austenitização de componentes de grandes dimensões, é inevitável a existência de um gradiente térmico. Isto deve-se ao facto de o centro da ferramenta aquecer a um ritmo mais lento, ao entrar na fase de austenitização, a superfície da ferramenta regista um tempo de estágio mais longo do que o centro. Se a austenitização ou o revenido começarem a uma temperatura alguns graus Celsius abaixo da temperatura desejada, é possível obter uma vantagem considerável no tempo total necessário para o tratamento térmico do componente, desde que a uniformidade da microestrutura e a dureza desejadas não sejam comprometidas. Foi utilizada uma combinação de procedimentos experimentais, incluindo a caraterização microestrutural e mecânica, com o objetivo de avaliar uma série de ciclos de tratamento térmico. Os ciclos de tratamento térmico foram selecionados com base na taxa de aquecimento da superfície e do centro, bem como no tempo de estágio normalmente requerido para este tipo de aço. Assim, o tempo de estágio mais frequentemente utilizado foi estabelecido como uma linha de base, a partir da qual foram selecionados diferentes tempos de estágio com base na temperatura a que se inicia a contagem do tempo. Os melhores resultados de têmpera foram obtidos quando se aplicou um ΔT de 20°C, resultando numa microestrutura martensítica com um mínimo de carbonetos não dissolvidos e uma dureza de 53 HRC $\pm$ 1 HRC para o centro e 46 HRC $\pm$ 1 HRC para a superfície da ferramenta, com austenite residual abaixo de 5 %. A aplicação do revenido triplo iniciado 20 ºC abaixo da temperatura desejada, resultou na formação de uma matriz martensítica temperada caracterizada por uma notável dispersão de carbonetos, incluindo carbonetos ricos em Fe, Mo e Cr. Esta modificação do tratamento térmico produziu igualmente uma dureza de 50 HRC $\pm$ 1 HRC e uma resistência ao impacto de 9 J $\pm$ 3 J, propriedades relacionadas com o centro da ferramenta. Em contrapartida, uma dureza de 44 HRC $\pm$ 1 HRC e uma resistência ao impacto de 15 J $\pm$ 1 J foram observadas para a superfície da ferramenta. Os resultados demonstram o impacto da variação das condições de tratamento térmico na dureza, no tamanho do grão e na distribuição de carbonetos do aço. Os resultados oferecem informações valiosas para a otimização do processo de tratamento térmico do aço AISI H11 Premium, contribuindo para o desempenho das ferramentas em aplicações industriais.

Palavras-Chave: AISI H11 Premium, Dureza Rockwell-C, Melhoria, Precipitação de Carbonetos, Revenido, SEM/EDS, Têmpera, Tenacidade.

Acknowledgements

Em primeiro lugar, quero expressar a minha gratidão aos meus orientadores. À Professora Laura Ribeiro, pelo ensino dos conceitos fundamentais durante o meu percurso académico e pelo apoio, dedicação e orientação ao longo da elaboração deste trabalho. Ao Engenheiro Paulo Duarte, pelo suporte e disponibilidade oferecidos durante o projeto, e pelo conhecimento que fez sempre questão de transmitir e ensinar.

Agradeço ao Sr. Ramiro, à D. Cândida, à Engenheira Cláudia, à Professora Aida, à Professora Sónia e ao Engenheiro Fecheira por todo o suporte crucial para a conclusão bem sucedida do projeto. Agradeço, também, ao Bernardo, ao Hélder e à Beatriz pelas conversas no laboratório e pela orientação quando eu precisava de ajuda. Um obrigada ao Ivo por me ter ensinado a trabalhar com ferramentas fundamentais para a realização desta tese.

Um agradecimento, do fundo do coração, aos grandes amigos que levo daqui, a todos os que sabem o que significa fazer um *takeover* à grande cidade da Guarda, aos mais dinâmicos (e flexíveis), aos maiores trabalhadores da emprezza, sem vocês esta jornada não seria igual.

Ao Duarte, por ter estado ao meu lado ao longo de mais uma etapa, pelo permanente incentivo, preocupação e cuidado que me proporcionaram suporte para finalizar este projeto.

Um profundo obrigada à minha família, aos meus pais, à minha avó, à Catarina e ao Ricardo, que tornaram tudo muito mais fácil com todo o apoio que me deram ao longo desta etapa, por todas as conversas, pelo incentivo e carinho que demonstraram sempre e se tornaram essenciais para continuar. E, por fim, mas não menos importante, um obrigada aos meninos, ao Felício, à Bambina, à Pantera e ao Miquelino, sem eles não sei o que seria de mim.

Obrigada.

Isabel Miranda

"There's no need to rush.
Please take your time to polish your talent."

Shirou Nishi, *Whisper of the Heart*

Contents

List of Figures

List of Tables

Abbreviations

CCT Continuous Cooling Transformation

CVN Charpy-V Notch Impact Test

EDS Energy-Dispersive X-ray Spectroscopy

FCC Face-Centred Cubic

NADCA North American Die Casting Association

OM Optical Microscopy

SEM Scanning Electron Microscopy

TEM Transmission Electron Microscopy

XRD X-Ray Diffraction

Chapter 1

Introduction

This chapter provides an overview of the study area and emphasises the significance of accurately parameterising the heat treatment of hot work tool steels to minimise time and costs, while still meeting the required mechanical properties. The chapter also addresses the motivation and the scope of the work, problem definition, objectives, as well as the impact of this research on the heat treatment industry.

1.1 Motivation and Strategy

Heat treatment is a crucial step in producing moulds for hot work applications. Indeed, the three main factors that affect tool life are the material of the die, its heat treatment, and the control of the die casting process. The die material usually represents 5 % to 15 % of the total die cost, while heat treatment costs around 5 % to 10 % [1]. Moulds for hot work applications require a significant investment, and heat treatment is a costly stage in mould production. This concerns designers, purchasers, suppliers, heat-treaters, mould makers, and die-casters. Heat treatment is one of the most important factors for the success of mould production, whether for plastic-injection moulding or aluminium casting. Traditionally, manufacturers customise dies and moulds to produce high-quality products with advanced features that extend their lifespan. The quality of these tools is crucial as it directly affects the performance of the final product. Therefore, manufacturers are often required to invest significant resources in the production of complex and durable dies and moulds [2, 3, 4] .

The critical heat treatment of hot work tool steels is necessary due to their high demand applications. Thus, the appropriate heat treatment is crucial to achieve the desired mechanical properties

of hot work tool steels. This involves austenitising and quenching and, afterwards, tempering. To achieve the required secondary hardening, the alloying elements must be in solid solution in the as-quenched structure, typically martensite. This can only be achieved through adequate austenitising time and temperature for hardening, which dissolves the alloy elements present in the form of carbides in the initial annealed state. Excessive grain growth should be avoided. Finally, tempering should eliminate retained austenite and promote adequate precipitation of the alloy carbide [2, 5]. Time and temperature are crucial factors in the heat treatment of hot work tool steels and require careful selection. The austenitisation stage is characterised by a longer holding time for the surface of the tool in comparison to the centre. This phenomenon can be attributed to the existence of a thermal gradient, whereby the surface heats at a faster rate than the centre. The commencement of austenitisation or tempering at a temperature that is a few degrees Celsius below the desired temperature allows for considerable savings in the total time required to heat treat the component, provided that the desired microstructure uniformity and hardness are not compromised. The aim is to decrease the duration of the heat treatment cycle while maintaining the desired properties of the material and, consequently, the component's performance. Despite the existing literature, further research is required to fully understand the effect of process parameters on the microstructure of the AISI H11 Premium hot work tool steel. This understanding will help determine the microstructure's influence on toughness, hardness, and ultimately, component performance. This study proposes a novel heat treatment methodology for AISI H11 Premium tool steel, which considers the thermal gradient between the surface and the centre of the tool. This approach results in a reduction in time (Δt), cost and environmental impact, and includes microstructural characterisation, which is crucial for understanding the material's hardness and toughness.

This project represents a collaborative endeavour between the company MetalSolvus and the Department of Metallurgical and Materials Engineering (DEMM) of the Faculty of Engineering of the University of Porto (FEUP). MetalSolvus provides consultancy services to the heat treatment industry, and thus the project was developed on the basis of industrial experience, specifically in the heat treatment of AISI H11 Premium steel.

1.2 Objectives and Contributions

The aim of this study is to propose an alternative heat treatment cycle for large hot work tool steel moulds that can reduce both time and cost while still achieving the required properties. The aim of this study is to investigate the impact of the thermal gradient between the surface and the centre of the tool and the start of the austenitisation and tempering time at a temperature below the desired temperature on the AISI H11 Premium microstructure and mechanical properties. This will enable a determination

to be made as to the suitability of the heat treatment cycles for use in the heat treatment industry. A detailed examination of the heat-treating curves (heating, stage and cooling) employed in the heat-treatment industry has revealed that the typical curves exhibit a relatively high heating rate at the outset, which then declines significantly as the temperature approaches the desired temperature. This decline typically occurs within a time range equivalent to approximately one-third of the total time allotted for the stage, as illustrated in Figure 1.1. This phenomenon was observed in both quenching and tempering processes. Two approaches were undertaken to investigate this phenomenon further: one for quenching and another for tempering.

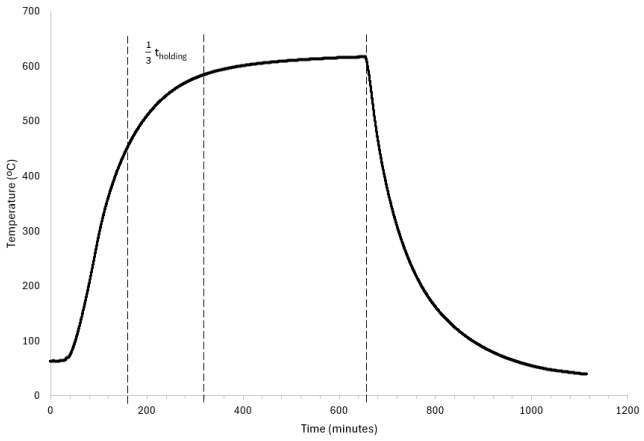

Figure 1.1: Representation of the typical behaviour observed in a heat treatment cycle curve.

Three conditions were defined for the austenitising process. The first employed the conventional heat treatment, with the holding time occurring at the desired temperature. The second involved a part of the holding time at 10 ºC lower than the desired temperature. The third displayed a part of the holding time at 20 ºC below the desired temperature. In consideration of the centre of the tool as the most critical section, subsequent statements will pertain to this area. The phenomenon observed in the typical heat-treating curves (Figure 1.1) can be translated and simplified into a step at a temperature a few degrees Celsius from the desired temperature. This step will account for a third of the total tempering time, thereby allowing us to study the material performance when a third of the total tempering time is spent at 550°C and 540°C, with a ΔT of 10°C and 20°C, respectively.

Therefore, the main contribution of this thesis is the development of a heat treatment cycle well suitable for the AISI H11 Premium tool steel, permitting a adequate component's performance with a reduction in time, cost and environmental impact for the heat treatment industry. Furthermore, this project contributes to the Sustainable Development Goals, as outlined in Table 1.1.

Table 1.1: Sustainable Development Goals

SDG	Definition	Target Indicators
9. Industry, Innovation and Infrastructure	Build resilient infrastructure, promote inclusive and sustainable industrialization and foster innovation.	9.4. Increased resource-use efficiency; 9.5. Enhance scientific research, upgrade technological capabilities of industrial sectors in all countries and encourage innovation.
12. Responsible Consumption and Production	Ensure sustainable consumption and production patterns	12.6. Encourage companies to adopt sustainable practices and to integrate sustainability information

1.3 Structure of the Thesis

The thesis comprises five chapters, each briefly described in this overview section.

Chapter 1 describes the context of the study area and emphasises the significance of developing a new heat treatment cycle for the AISI H11 Premium hot work tool steel. The chapter also covers the motivation, problem definition, objective, and impact of this research on the heat treatment industry.

Chapter 2 contains the literature review on the heat treatment of AISI H11 hot work tool steel. The review provides an overview of effect of heat treatment parameters on the microstructure and mechanical properties, including hardness, tensile behaviour, and toughness of the tempered AISI H11 Premium steel. The chapter is divided into two sections. The first section covers the material, its properties, and its applications. The second section discusses the heat treatment of this type of hot work tool steel, including quenching and tempering.

Chapter 3 focuses on the experimental procedure. It includes material composition, heat treatment cycles, methodologies, and technologies used to perform microstructural characterisation. Additionally, it provides details of the mechanical properties tests, such as the hardness test, tensile test, and impact test.

Chapter 4 presents the main results of the experimental work described in the previous chapter and as well as a comprehensive examination of the research findings with a particular focus on the most noteworthy outcomes. The chapter is divided into three sections. The first section covers the microstructural characterisation of the annealed state of the AISI H11 Premium steel. The second section is devoted to the quenched samples. Finally, the third section includes the results related to the quenched and tempered samples. This chapter presents a correlation between the findings and the conclusions derived from them, as well as an analysis of the implications of these conclusions.

Chapter 5 presents the conclusions of the research on the influence of heat treatment parameters on the microstructure and mechanical properties of AISI H11 Premium steel. Recommendations for

future work in this field are also provided.

Chapter 2

Literature Review

This chapter presents a literature review on the heat treatment of hot work tool steels, specifically quenching and tempering of AISI H11 Premium. The focus is on carbide precipitation and the influence of altering the thermal cycle parameters on mechanical properties. Additionally, the chapter includes a discussion on the importance of quality in heat treatment and its impact on the final performance of the component.

2.1 Hot Work Tool Steels

Hot work tool steels are a family of special tool steels designed for parts that come into contact with hot metals for varying periods, with or without cooling. They are specifically developed for regular use in these conditions [6]. Steels for hot-work applications are designed to maintain their strength and hardness even after prolonged exposure to high temperatures, which is necessary for hot-working or die-casting other materials. The history of tool steels has seen significant developments. Hardened steel was first documented in 1200 BC. The earliest tool steels were simple, unalloyed carbon steels, but from 1868, and to a greater extent in the early 20th century, many complex, high-alloy tool steels were developed, achieving greater dimensional control and freedom from cracking during heat treatment. In 1904, alloys were improved by adding 0.4 % vanadium, and in 1912, the addition of 3 to 5 % chromium resulted in hot hardness tool steels, which can resist softening during long or repeated exposures to high temperatures. In 1992, 8 % Cr tool steels were created, resulting in high toughness [7, 8]. Finally, in 2000, low-silicon hot work tool steels were developed [7]. Designated as Group

H steels in the AISI classification system, this type of steel can be subdivided into chromium hot-work steels, tungsten hot-work steels, and molybdenum hot-work steels. Multiple alloying elements are added to improve performance [2]. Chromium hot-work tool steels are characterised by their chromium content, which imparts high hardenability, excellent toughness, and great ductility, albeit at the expense of wear resistance. H1 to H19 hot work steels are referred to as chromium types, although other significant alloying elements may be present. H10 to H13, the molybdenum-containing types, are the most widely used of all hot work steels and are characterised by high hardenability and outstanding toughness [5, 6]. Tool steel selection begins with the identification of the group or groups of tool steels that best satisfy the requirements of a given application. Although the hot hardness of chromium types is lower than that of tungsten and molybdenum hot work tool steels, the high shock resistance makes these type of hot work tool steel more suitable for most hot-work operations. This is particularly relevant when dies require water-cooling or cooling with other flushing media. Furthermore, when it comes to this type of operation, chromium hot work tool steels are preferred over molybdenum hot work tool steels due to their higher ductility [6, 9].

Hot work tool steels are primarily used in metal forming processes that require temperatures above 600 ºC. These processes include steel forging, extrusion, and casting of nonferrous alloys, such as aluminium alloys. Additionally, they can be applied in moulds for plastic injection moulding. In this context, it is necessary to have properties such as high strength at elevated temperatures, shock resistance, and resistance to thermal and mechanical fatigue [2, 5, 7]. Hot-work tool steels are differentiated from other tool steels by their ability to resist deformation at high working temperatures. This mechanical strength is crucial in preventing softening at high temperatures and is related to tempering resistance, which allows for the maintenance of hardness over prolonged periods at high temperatures. Higher tempering resistance is indicated by tempering curves that are shifted to the right, as it can be verified in Figure 2.1, where the tempering curve of VHSUPER (AISI H11 Premium) is on the right of that of AISI H11. Additionally, these steels require shock resistance to prevent cracking and catastrophic failure. In situations where the material lacks toughness, it may experience gross cracking. To achieve resistance to heat treatment distortion, it is best to use higher-alloy steels with sufficient hardenability to allow for hardening through air cooling. The life of hot-work tool steels is mainly affected by resistance to heat checking, which refers to networks of fine, shallow cracks that develop due to repeated exposure to cycles of heating and stress. This has an impact on the surface quality of the final component after casting [2, 5]. Hot-work tool steels typically have a lower carbon content than cold-work tool steels, resulting in lower hardness after quenching and lower abrasive wear resistance due to the reduced presence of undissolved carbides. Final hardness is usually determined by desired toughness rather than wear resistance, typically ranging between 40 and 50 HRC. As previously stated, the main metallurgical properties are toughness and strength at high temperatures, which

are highly dependent on the stability of hardness at high temperatures [5].

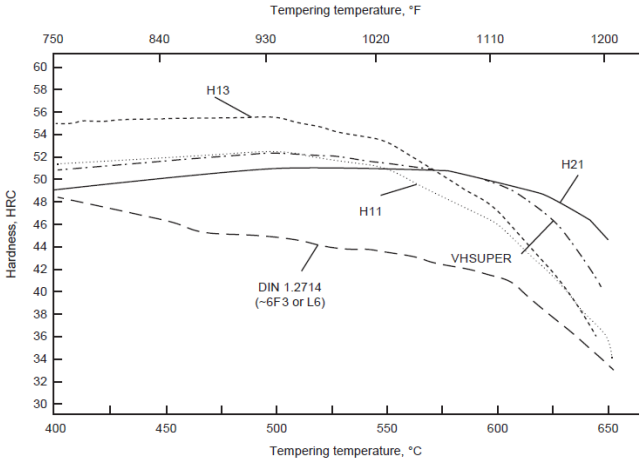

Figure 2.1: Tempering curves for AISI H11 and AISI H11 Premium (VHSUPER) obtained after hardening 25 mm speciments at 1020 ºC [5]

2.1.1 AISI H11 Premium

AISI H11 (0.37 %C, 1.00 %Si, 0.35 %Mn, 5.15 %Cr, 1.30 %Mo, 0.40 %V and remaining Fe [10]) is a popular and relatively economical hot work grade with many applications. This material is deep hardening and has excellent resistance to heat checking, which is particularly important in die casting and other hot working processes where cracking is likely to occur. New hot work tool steels have been developed based on existing tool steels, such as the AISI H11 Premium tool steels low sulphur and phosphorus steel grades, which, as the name suggests, are based on the composition of H11. These steels are usually known by their brand name, as with Uddheholm Vidar Superior or W400 from Boehler (AISI H11 Premium) (0.37 %C, 0.25 %Si, 0.30 %Mn, 5.15 %Cr, 1.25 %Mo, 0.45 %V and remaining Fe [10]) [5, 11, 12].

Modifying the concentration of alloying elements that are directly involved in the precipitation of secondary carbides is the most conventional method of improving tool steel properties. This is because it shifts the secondary hardening peak towards higher temperatures as previously observed in Figure 2.1. The influence of steel composition on austenitising and tempering temperatures is significant. There are two categories of alloying elements: carbide-forming elements, such as Mo, V, W, and Nb, and elements that only modify the tempering kinetics, such as Co and Si. The modified AISI H11 is characterised by a reduced Si content, typically from 1.0 % to 0.3 % or lower levels [13]. Reducing the silicon content leads to higher toughness and resistance to heat checking, which is crucial in meeting the growing demands for tool life and it also significantly improves wear resistance.

The steel AISI H11 has been modified to exhibit improved tensile and fatigue properties above 550 ºC, which is the estimated tool surface temperature during high-pressure injection of aluminium alloys. Si presents the ability to retard the formation of cementite during the early tempering stages resulting in increased tempering resistance, as it leads to significant changes in the nature and distribution of the final secondary alloy carbides. High Si steels delay or inhibit cementite formation, leading to alloy carbide formation with preferred M_7C_3 precipitation on high-energy interfaces. However, after long tempering, these particles may coarsen and act as preferential cracking routes, resulting in lower toughness. On the other hand, for low Si steels, carbon is stabilised by Cr, Mo and V in solid solution, delaying alloy carbide formation and increasing tempering resistance. As these changes improve toughness properties under optimised heat treatment conditions, the requirements for process control also increase, especially for large dies [5, 13, 14, 15, 16].

2.2 Quenching and Tempering

This section includes a literature review on austenitisation, quenching and tempering of hot work tool steels, specifying on the phenomena that takes part when heat treating AISI H11 Premium. Properly heat-treated hot work tool steel has an optimal distribution of fine carbides in a tempered martensite matrix, producing good hot hardness. Heat-checking is a well-known factor that limits the lifespan of hot-working tools. Chromium hot-work tool steels with good heat-checking resistance are produced by heat-treated microstructures that exhibit good hot hardness and toughness. It is important to note that microstructure plays a crucial role in determining the optimal properties of the steel. To achieve the desired toughness and hardness levels, it is preferred to have a fine grain size and finer microstructural characteristics such as martensitic plates and carbide particles in the hot work tool steel. It is imperative that the correct alloy composition and microstructure are maintained on the surface of hot work tooling and dies during processing and, in particular, that surface decarburisation or carburisation is minimised during austenitisation for hardening [2].

2.2.1 Austenitisation

Austenitisation is the step of the heat treatment for dissolving carbon into the austenitic phase. At the end of this step, the final alloy element partitions between the austenitic matrix and the retained carbides. The partitioning process determines the chemistry, volume fraction, and dispersion of the retained carbides. The alloying elements that are not bound up in retained carbides are in solution in the austenite, hence the carbides play a significant role in stabilising austenite decomposition during subsequent cooling. Thus the austenite composition determines the hardenability, the M_s temperature,

the retained austenite content, and the secondary hardening potential of tool steel. In this sense, austenitising is one of the most important steps of all heating procedures in tool steels and must be closely managed [8, 17].

- **Heating**: Heating is an important step when heat treating a part. The centre of the tool must not be cooler than the exterior when heating, as it can result in insufficient or absence of austenitisation, and the surface must be free of decarburisation. Preheating or slow heating of tool steels before austenitising is a good practice, although it is not always necessary, as in the case of small components with simple shapes. This method is frequently undertaken to protect against the cracking and excessive deformation caused by the thermal shock experienced by a cold workpiece when exposed to the high temperature of the austenitising furnace [8] . Typically, two pre-heating steps are performed for AISI H11 Premium, the first at a temperature between 600 and 650 ºC and the second between 820 and 850 ºC [18].
  - **Heating medium:** The heating medium is crucial in protecting against carburisation or decarburisation. When using a controlled atmosphere, the protective gas can be exothermic, endothermic or inert. Furthermore, vacuum hardening has become increasingly popular and is now the most common method for hardening hot work tools. The process involves placing the charge in a cold furnace, which is then evacuated using vacuum pumps. Once the charge has been heated and austenitised under inert atmosphere, the furnace charge is cooled to room temperature, typically using a nitrogen (most common inert gas) atmosphere blowing. The main advantage of vacuum hardening is that the surface remains unaltered, avoiding carburisation or decarburisation. Furthermore, it can reduce production time and costs [17]. Among these, the recommended atmospheres for AISI H11 Premium are vacuum or endothermic atmosphere [18].
- **Temperature:** For hardening each grade of steel, a specific range of temperatures must be considered for heating and it is selected to achieve maximum hardness while maintaining a fine-grained structure in the steel. The dissolution of carbides is determined by the temperatures used during heat treatment, as well as the potential for achieving certain grain sizes and other microstructural features, such as retained austenite and martensite plates. On the one hand, exceedingly high austenitising temperatures or arbitrarily lengthy holding times can cause severe deformation, unusual grain growth development, retained austenite, and, consequently, loss of hardness and strength. On the other hand, underheating can result in low hardness and wear resistance as the matrix cannot be fully austenitised, preventing complete transformation into martensite. Martensite is the phase responsible for hardness and wear resistance. Figure 2.2

presents information related to AISI H11 Premium, showing that as the austenitisation temperature increases, both grain size and hardness increase for the same period [17, 18]. It can be demonstrated that an increase in the austenitising temperature results in grain growth and, consequently, a reduction in the number of grain boundaries. This facilitates the decomposition of austenite into martensite, accompanied by an increase in carbon content within the austenitic matrix. Consequently, when quenched, martensite with a higher carbon content will result in an increase in hardness [19]. Austenitising temperature for the AISI H11 Premium steel can be found between 980 and 1000 ºC. In fact, when compared to AISI H11, for this modified version, austenitising temperatures are slightly reduced and strictly controlled to avoid grain coarsening [5, 18].

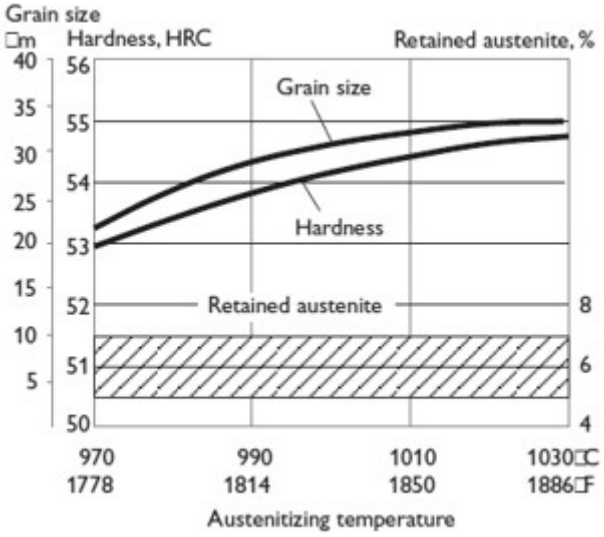

Figure 2.2: Effect of austenitising temperature on hardness and grain size of AISI H11 Premium specimen [18].

- **Holding time:** When the steel reaches the hardening temperature, the holding time depends on the desired degree of carbide dissolution and the grade of steel being treated. Hot-work steels contain carbides that do not dissolve until approximately 1000 ºC. At these high temperatures, grain growth is rapid, so the holding time must be limited. When packing the parts in a box for heat treatment, it is recommended to use the temperature at the lower limit of the austenitisation range. This allows for a longer holding time. Diagrams displaying data on grain size, hardness after hardening, and the amount of retained austenite should be included to show the interrelation between holding time, hardening temperature, and carbide dissolution. Figure 2.2

presents information related to AISI H11 Premium, showing that as the austenitisation temperature increases, both grain size and hardness increase [17]. The holding times for this type of steel typically range between 30 and 45 minutes. However, the required holding time is strongly influenced by the dimensions of the part being treated. A greater thickness demands a longer holding time. For example, a holding time of 30 minutes is required for a thickness of 1 inch, and for each additional inch, the holding time must be increased by 15 minutes [18, 20]. When heat treating a part or a charge, the holding time is typically selected based on centre austenitisation, which results in a significantly longer time for the surface. This unavoidable procedure leads to a microstructure for the surface that is always different from that of the centre. As a result, steel tools will have different mechanical properties after the heat treatment.

2.2.2 Quenching

Quenching can be defined as the rapid cooling of the steel from a temperature above its critical temperature (A_3 temperature) in a medium such as oil, water, brine or even air. The aim is to obtain the martensitic structure and therefore the cooling curve must pass on the left bend of the Continuous Cooling Transformation (CCT) curve, thus preventing the transformation of austenite into ferrite, pearlite and carbides. The alloying elements in hot work tool steels generally increase the possibility of martensite formation, so it is possible even if cooling is not very rapid. In high-alloy steels, martensite can be obtained even with air cooling, so it is said that alloying elements increase hardenability [7, 8]. When hardening hot work tool steel, the goal is typically addressed to achieve a bainitic-martensitic structure. Therefore, the cooling rate must be controlled to prevent the formation of pearlite [17].

Based on the literature, nitrogen gas or air cooling is recommended as the appropriate quenching medium for AISI H11. For the modified low-silicon H11, hardness values of 53 to 55 HRC are expected after quenching. AISI H11 Premium requires higher critical cooling rates to avoid bainite formation, therefore even higher rates of cooling are recommended compared to standard grades. The minimum cooling rate suggested is 28 ºC/min. Parts thicker than 12.7 cm (5”) may not achieve full hardness with air quenching and may require oil quenching [5, 18, 20, 21].

2.2.3 Tempering

Tempering is a crucial step in the heat treatment of hot work tool steels. It follows quenching and aims to eliminate most of the disadvantages that arise from the martensite in steels. Martensite can exhibit high hardness, but in the untempered state, it is rather brittle. It is mainly driven by the fact that martensite is not an equilibrium phase. It is therefore necessary to mitigate this difficulty by

heat treatment in the range of 550ºC to 700ºC. It corrects the excessive hardness and brittleness of the material, increases ductility and impact resistance and is also responsible for relieving and eliminating internal stresses. The aim is to achieve a good combination of strength and toughness. The mechanism of tempering presupposes the thermally activated approach to equilibrium, by redistribution of carbon or its precipitation, the rearrangement or elimination of crystal defects and the relief of stresses [7, 8, 22]. The typical tendency during martensite tempering begins with the rejection of excess carbon, which precipitates carbides. Tempering produces a dispersion of coarse carbides in a ferritic matrix with little similarity to the original martensite. To achieve an ideal microstructure, more than one tempering cycle may be required, and it is usually preferable to transform all residual austenite to ensure complete hardness, increase toughness, and reduce distortion in service, which can be accomplished more efficiently with two or three shorter tempering cycles than with a single longer cycle. This is accurate because the number of heating and cooling cycles applied to the material is increased, thereby facilitating the destabilisation of the austenite and its transformation. During the cooling process after the first tempering cycle in higher-alloy tool steels, a small quantity of untempered martensite is generated from residual austenite. This suggests the necessity to double temper to get a more nearly complete transformation. In some circumstances, a third and fourth cycle is recommended [8]. According to this definition, tempering can be divided into four overlapping temperature ranges:

1. **First Temperature Range:** Martensite formed in medium and high-carbon steels (0.3 to 1.5 wt% C), as in the case of AISI H11 Premium (0.37 wt%C), is unstable at room temperature due to the diffusion of interstitial carbon atoms in the tetragonal martensite lattice. The distribution of carbon becomes more unstable between room temperature and 250 ºC, leading to the precipitation of ε-iron carbide, which is represented by the $Fe_{2\text{-}3}C$ formula and a close-packed hexagonal lattice. This carbide precipitates as narrow plates in the matrix, with a well-defined orientation relationship. At the end of the stage, the martensite still possesses a tetragonality, although it may be partially lost, indicating a carbon content of around 0.25 wt%. Other transition carbides may also precipitate. Excess carbon in the martensite may slowly partition into residual austenite, because of the lower free energy of carbon within the austenite. A decrease in Rockwell hardness is observed [7, 22].

2. **Second Temperature Range:** Retained austenite, which is present after quenching, typically decomposes in the temperature range of 230 to 300 ºC. According to the available literature, this decomposition results in the formation of bainitic ferrite and carbides [7, 22].

3. **Third Temperature Range:** Cementite initially appears in the microstructure as a Widmanstätten distribution[1] of plates. These plates have a well-defined orientation relationship with the matrix, which has lost its tetragonality and become ferrite. This reaction begins at temperatures as low as 100 ºC and is fully developed at 300 ºC. Martensite lath boundaries also serve as a site of nucleation. The addition of alloying elements, as in the case of AISI H11 Premium, prevents cementite formation as thin films that gradually spheroidise into well-defined particles in the grain boundary regions, avoiding its detrimental effect on ductility. Eventually, the tetragonality of the matrix disappears, but, for AISI H11 Premium, the tetragonal lattice is still observed after tempering at 450 ºC and even as high as 500 ºC. Subsequent changes in the morphology of cementite particles occur through an Ostwald ripening process, where smaller particles dissolve in the matrix, providing carbon for the selective growth of larger particles. Rockwell hardness continues to decrease [7, 22].

4. **Fourth Temperature Range:** The process of cementite coarsening can be influenced and limited by the presence of alloying elements, such as chromium, silicon, and molybdenum. This phenomenon occurs within the temperature range of 500 to 600°C and is a fundamental process during the fourth stage of tempering. It is important to note that up to 500°C, only carbides of iron form. In this context, cementite keeps its Widmanstätten structure and this leads to a significant delay in the softening process. There is the precipitation of alloying carbides which are more thermodynamically stable than cementite, and the transformation is called 'secondary hardness'. This is a typical phenomenon of medium and highly Cr-Mo-V alloyed steels, such as AISI H11 Premium, known as secondary hardening. It is a type of age-hardening reaction where a relatively coarse cementite dispersion is replaced by a new and much finer alloy carbide dispersion. It occurs between 500 and 550 ºC and involves two processes: the transformation of retained austenite into martensite during cooling and tempering, and the precipitation of an extremely fine dispersion of carbides of alloying elements. Alloy carbides do not form until the temperature range of 500 ºC to 600 ºC because, below this temperature, the metallic alloying elements cannot diffuse rapidly enough to allow for the nucleation of alloy carbides. The elements Cr, Mo, and V all form carbides with significantly higher enthalpies of formation. Mn is a weak carbide former and is present in a solid solution in cementite rather than a separate carbide phase. Nucleation and growth of alloy carbides can be expressed in a complex way, but some general principles explain their behaviour. The alloy carbides can form, essentially, in three ways:

[1] The Widmanstätten structures form as a result of new phases growing within the grain boundaries of the parent metals. This generally increases the hardness and brittleness of the metal. The structures form due to the precipitation of a single crystal phase into two separate phases.

- *In-situ* nucleation at pre-existing cementite particles: it occurs in the interfaces between the cementite particles and the ferrite. As the alloy carbides grow, carbon is provided by the adjacent cementite which gradually disappears.
- By separate nucleation within the ferrite matrix: usually on dislocations inherited from the martensite structure
- At grain boundaries and sub-boundaries: these may be the former austenitic boundaries, the original martensitic lath boundaries, that turned into ferrite, and the new ferrite boundaries formed by coalescence of sub-boundaries, or by recrystallisation [7, 22].

The tempering curve of AISI H11 Premium, previously austenitised at 980 ºC and 1000 ºC, observed in Figure 2.3 begins at moderate hardness levels, consistent with the as-quenched martensitic hardness. Small hardness peaks at approximately 540 ºC indicate secondary hardening, as explained in the fourth stage of tempering. Tempering beyond peak hardness is performed to avoid the minimum toughness that develops when the chromium hot work steels are tempered at temperatures that produce peak strengthening. This corresponds to an overaged or overtempered condition.

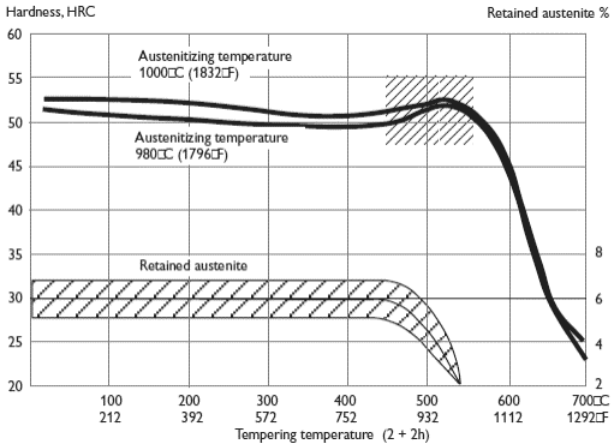

Figure 2.3: Tempering temperature vs Hardness of AISI H11 Premium specimen 15 x 15 x 40 mm [18] [Uddeholm].

The tempering behaviour and carbide precipitation of AISI H11 Premium are significantly influenced by its alloying elements and heat treatment parameters, such as austenitising temperature, tempering temperature, and time.

- **Influence of Parameters:**
  - **Austenitising Temperature:** Increasing the austenitising temperature reduces the room temperature impact toughness in specimens treated at temperatures of 595 and 620 ºC,

which are above those that produce peak hardness. This reduction is due to a transition to intergranular fracture along prior austenite grain boundaries, caused by greater susceptibility to carbide formation on austenitic grain boundaries in specimens austenitised at higher temperatures [2, 5, 18]. In addition, the austenitising temperature significantly impacts hardness, as it has a proportional relationship. Increasing the austenitising temperature promotes carbide dissolution, making the alloying elements necessary for hardenability and eventual secondary hardening available. However, increasing the austenitising temperature has implications on grain size and retained austenite [7, 22]. Podgornik *et al.* reported that raising the austenitising temperature from 990 to 1030 ºC resulted in an increase in grain size and martensitic lath size, as well as a higher number of secondary carbides [14]. Leskovsek *et al.* investigated the impact of austenitising and tempering temperature on the mechanical properties of hot-work H11 tool steel. The author found that the highest fracture toughness was achieved at an austenitising temperature of 1020 ºC and double tempering across the entire range of tempering temperatures used [23]. Podgornik *et al.* reported that an increase in austenitising temperature led to increased dissolution of the primary carbides. However, the latter parameter may increase austenite grain size and carbide particles coarsening and it leads to a drop in fracture toughness [24]. Additionally, austenitising at high temperatures in the hardening range enhances grain-boundary carbide formation on cooling. This is due to the coarsening of austenitic grain size and the increased carbon that goes into solution as the alloy carbides dissolve. It is important to note that the presence of grain-boundary carbide networks increases the susceptibility of H-type steels to brittle intergranular fracture [2].

– **Tempering Temperature:** Bibliography suggests that the highest hardness values are achieved for tempering temperatures between 500 and 550 ºC. However, tempering in the temperature range of 450 to 550 ºC results in the lower toughness [2, 5, 18]. Podgornik *et al.* reported that an increase in the tempering temperature led to intensified precipitation and up to four times more fine secondary carbides. This had an impact on the mechanical properties of the tool steel, hardness decreased and toughness increased with an increase in tempering temperature [14]. Podgornik *et al.* concluded that an increase in tempering temperature resulted in an increased volume fraction of precipitated secondary carbides [24]. Mebarki *et al.* observed that an increase in the second tempering temperature resulted in a decrease in the dislocation density. Additionally, the author found that an increase of the weight fraction of carbides is observed for tempering temperatures above the secondary strengthening peak around 550 ºC [25]. Dandekar and Khatirkar investigated the effect of tempering temperature on the abrasive wear of AISI H11 steel. The

samples tempered at 200 ºC contained martensite, retained austenite, and a small number of carbides due to insufficient diffusion time. On the other hand, samples tempered at 400 and 600 ºC showed a rise in the number of secondary carbides and a decrease in the volume fraction of retained austenite. The study revealed that the decrease in volume fraction of retained austenite led to an increase in the number of secondary carbides. As the tempering temperature increased, a reduction in hardness was observed [26].

- **Tempering Time:** Lerchbacher *et al.* investigated a novel technique for tempering AISI H11 steel and its impact on retained austenite. The study found that reducing the dwell time during the initial tempering stage can prevent direct decomposition of retained austenite into ferrite and cementite. This is because the austenite transforms into martensite before being tempered. However, for low quenching rates, direct decomposition is favourable as the new method of indirect decomposition leads to toughness degradation. Furthermore, reducing the dwell time during the first tempering stage results in a second significant nucleation and growth period during the second tempering stage, which could have a positive effect on the morphology and distribution of secondary carbides. The impact toughness is increased by 12 % with a 15 % reduction in dwell time due to the modified heat treatment. This method could be used to produce small tools [27].

- **Influence of Alloying Elements:** The modified AISI H11 steel contains 4.80 - 5.50 % chromium, 1.10 - 1.40 % molybdenum, and 0.30 - 0.60 % vanadium.

  - **Chromium:** In chromium steels, Cr_7C_6 (trigonal) and $Cr_{23}C_6$ (cubic) are often encountered and the normal sequence starts with the matrix, then precipitation of M_3C, followed by M_7C_3 and finally $M_{23}C_6$, in which M represents a mixture of iron and chromium atoms, although the last two are chromium-rich. For chromium steels below 7 wt% Cr, $Cr_{23}C_6$ is absent, unless other metals such as molybdenum are present. Chromium diffuses quickly in ferrite and is typically found in high concentrations. As a result, Cr_7C_3 is detected during tempering at around 500 ºC and coarsens rapidly [2, 5, 7, 18, 22].

  - **Vanadium:** Vanadium has minimal influence on hardenability due to their incorporation in stable alloy carbides and it is the key element for secondary hardening and tempering resistance. It is dissolved during austenitising for hardening and precipitates as very fine particles of vanadium-rich MC carbides in martensite laths, resulting in peak temperature hardness. Vanadium is a strong carbide former, and in steels with as little as 0.1 wt% V, the Face-Centred Cubic (FCC) vanadium carbide (VC) is formed. This carbide is frequently V_4C_3, but it may contain other elements in solid solution. Typically, this is the only vanadium carbide formed in steel, and its structural changes are relatively simple. Vanadium

carbide has a morphology of small platelets, typically less than 5 nm in size and with a thickness of less than 1 nm. These platelets form within the ferrite grains on dislocations between 550 and 650 ºC and have a significant impact on the secondary-hardening peak. Many steels containing vanadium exhibit extensive precipitation of vanadium carbide upon tempering due to the stability of this carbide. Vanadium plays an important role in elevated temperature service due to its ability to maintain a fine carbide dispersion at high temperatures, around 700 ºC. Vanadium is a stronger carbide former than chromium [2, 5, 7, 18, 22].

- **Molybdenum:** Molybdenum significantly promotes martensite formation at slower cooling rates. The addition of Mo can slow down the rate of coarsening. The isomorphous hexagonal carbide Mo_2C is responsible for secondary hardening. It has a well-defined rodlet morphology and, when formed in the matrix, assumes a Widmanstätten structure. This carbide nucleates at former austenite and ferrite lath boundaries and precipitates both on dislocations in the ferrite and at the cementite/ferrite interfaces. At lower concentrations of molybdenum (0.5 to 2 wt%), two other alloy carbides precipitate: the complex $M_{23}C_6$ and the orthorhombic M_aC_b, likely Fe_2MoC [2, 5, 7, 18, 22].

The presence of more than one carbide-forming element can make the precipitation process during tempering more complex. However, in general, the most stable thermodynamically will predominate, assuming that equilibrium is reached during tempering. The use of pseudo-binary diagrams for groups of steels can be useful in predicting the carbide phases that are likely to precipitate during tempering. However, it is important to mention that certain strong carbide formers, such as vanadium, have an effect out of proportion to their concentration. This element combines with carbon and forms a finer dispersion, is more resistant to over-ageing, is expressive in secondary hardening and presents significant relevance in achieving high strength levels at elevated temperatures [7, 22].

Research has been conducted to draw practical conclusions on the tempering of AISI H11 Premium. Podgornik *et al.* reported a fine needles like tempered martensite with uniform distribution of small secondary carbides, MC and undissolved primary carbides M_6C after quenching and double tempering at 560 ºC an AISI H11-low silicon hot-work tool steel. Microstructure shows no bainite or retained austenite, however, thin lamellar precipitates of M_3C type were observed between martensitic needles, which can be verified in Figure 2.4 [14]. Podgornik *et al.* reported fine needles of tempered martensite with a distribution of small secondary carbides and some undissolved eutectic carbides of M_7C_3 type, as well as a few thin lamellar precipitates of M_3C type between martensite needles after quenching and double tempering, as observed in Figure 2.5 [24]. Mebarki *et al.* observed laths

separated by elongated iron carbides in a specimen that was austenitised at 980 ºC, air-quenched, and double-tempered at 550 and 580 ºC. Four types of carbides were identified based on their morphology for all tempering conditions:

- facetted carbides: hexagonal Cr-Fe carbides (M_7C_3 type)
- large globular carbides (100 - 300 nm): FCC Cr-Fe carbides ($M_{23}C_6$ type)
- elongated carbides: Fe-Cr carbides (M_3C type)
- small globular carbides (<40 nm): FCC V carbides (MC type)

The precipitation sequence was detailed by the author using X-Ray Diffraction (XRD) and Transmission Electron Microscopy (TEM). The annealed steel contains M_2C (M: Mo mainly), M_3C (M: Fe mainly), $M_{23}C_6$ (M: Fe and Cr mainly) and a small amount of MC (M: V mainly). After quenching, only the vanadium carbide and small amounts of M_3C and $M_{23}C_6$ were found, due to their non-dissolution. After the first and second tempering, MC, M_3C, M_7C_3, and traces of $M_{23}C_6$ were present. The main carbides involved in the occurrence of the secondary hardening peak were defined as MC and M_7C_3. Two different populations of secondary hardening were identified after tempering: small carbides with an average size of 6 nm, that include vanadium and chromium carbides and carbides with an average size of 30 to 40 nm only found for second tempering temperatures above 600 ºC [25].

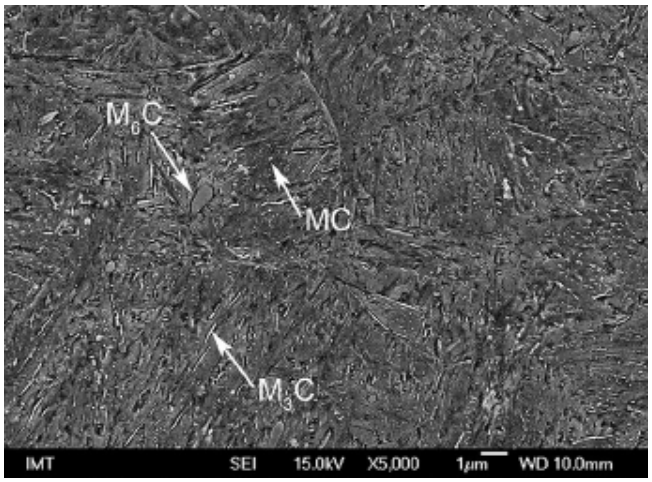

Figure 2.4: Microstructure of AISI H11 low silicon austenitised at 1000 ºC and double tempered at 560 ºC [14].

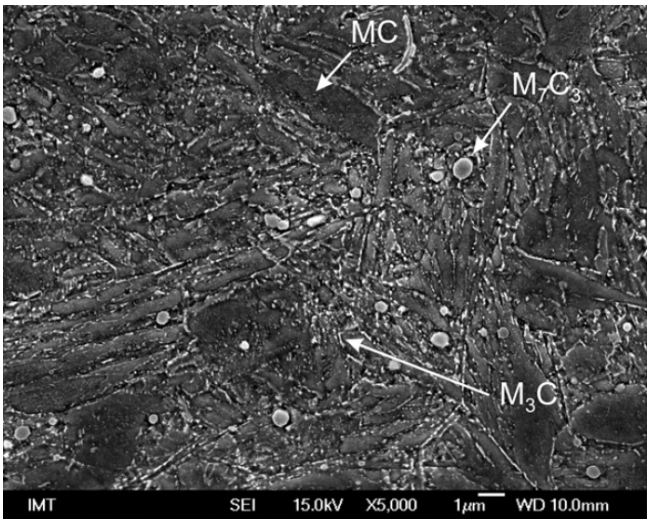

Figure 2.5: Microstructure of AISI H11 austenitised at 1000 ºC and double tempered at 630 ºC [24].

2.2.4 Hot Work Tool Steel Requirements

As mentioned in Section 1.1, the cost of heat treatment for a die is approximately 5 to 10 % of the total die cost. Quality assurance is crucial as it is a determining factor in the tool's lifespan [1]. Within this framework, properly performed heat treatment is crucial for the mechanical and operational properties of tools, as well as the economy of their use. Irregularities may lead to faster wear, deformation or defects and, in extreme cases, may lead to damage in the early stages of production and use [28]. As this type of steel is typically used for the production of moulds for die casting or plastic injection moulding, this section will focus on the requirements for this specific type of application.

North American Die Casting Association (NADCA) has released *Special Quality Die Steel & Heat Treatment Acceptance Criteria for Die Casting Dies* which provides one of the most advanced specifications for steel acceptance criteria and heat treatment [21, 29]. NADCA guidelines for heat treatment include the following criteria prior to heat treatment:

- Classifying steel grade with respect to the chemical composition of alloy additions and the contents of sulphur and phosphorus: NADCA specifies the category and composition comparison of special steel for die casting, which determines the basic properties of the material, which can be verified in Table 2.1;
- Measurements of hardness after annealing: When the mould material is delivered, it is important that its hardness in the annealed state is no greater than 250 HB. This ensures that the mould has good machining performance and microstructure;

- Analysis of the contents of micro-impurities: Microscopic analysis must be performed using a magnification of 100 times to observe the type and quantity of non-metallic inclusions in the steel, such as sulfides, aluminides, silicates, and globular oxides. It is important to note that the quantity of inclusions should be less than the specified limit according to ASTM E45;
- Checking internal defects: According to NADCA, ultrasonic inspection must be performed to prevent cracks, voids, and severe segregation. However, there are no specifications regarding the acceptable level of these issues;
- Defining grain size: According to NADCA, the ASTM E112 comparison method should be used to measure the grain size of die casting steel under a 100 times microscope. A grade of 7 or higher is required as it greatly influences the material properties;
- Examination of microstructure: The steel received must primarily consist of a ferritic matrix with a uniform distribution of spheroidised carbides. To evaluate the sample, it should be annealed, polished, and etched with a 5% nitric acid alcohol solution (5% Nital) before being observed under a microscope with a magnification of 500 times. NADCA offers an annealed microstructure rating chart to assess the sample's qualification [21].

Table 2.1: NADCA Grade Classification [21].

NADCA Grade	Material Category	C (%)	Mn (%)	P (%)	S (%)	Si (%)	Cr (%)	Mo (%)	V (%)
A	H13 Premium	0.37 - 0.42	0.20 - 0.50	0.025 max	0.005 max	0.80 - 1.20	5.00 - 5.50	1.20 - 1.75	0.80 - 1.20
B	H13 Superior	0.37 - 0.42	0.20 - 0.50	0.015 max	0.003 max	0.80 - 1.20	5.00 - 5.50	1.20 - 1.75	0.80 - 1.00
C	2367 & Modified	0.32 - 0.40	0.10 - 1.20	0.020 max	0.003 max	0.10 - 0.50	4.70 - 5.85	2.00 - 3.30	0.40 - 0.70
D	H11/ 2343	0.35 - 0.42	0.20 - 0.60	0.025 max	0.003 max	0.80 - 1.20	5.00 - 5.50	1.10 - 1.60	0.30 - 0.60
E	H11 Modified Superior	0.32 - 0.43	0.10 - 0.70	0.020 max	0.003 max	0.10 - 0.55	4.70 - 5.70	1.10 - 2.10	0.30 - 0.80
F	H11 Modified Premium	0.32 - 0.40	0.30 - 0.90	0.020 max	0.005 max	0.25 - 0.70	5.30 - 5.70	1.00 - 1.50	0.40 - 0.80
G	2367 Low Cr	0.32 - 0.40	0.10 - 0..60	0.020 max	0.003 max	0.10 - 0.50	3.50 - 4.00	2.00 - 3.30	0.40 - 0.70

Grade A is a general-purpose steel used in low-requirement fields. Grade B is also a general-purpose steel, but it requires secondary refining. Grade C is a high-toughness steel with high hardenability and tempering resistance, making it suitable for large-scale and long-life die casting moulds. Class D is suitable for large die casting moulds due to its high toughness, but it has lower wear and tempering resistance compared to classes A and B. Electro slag remelting is required for this grade. Grade E offers a performance level between that of grades B and C. According to these guidelines, AISI H11 Premium (Uddeholm Vidar Superior) is referred to as E1825 [21].

Based on NADCA criteria, heat treatment should be carried out in a vacuum furnace with high-pressure gas quenching while monitoring and controlling the surface and centre temperature using workload thermocouples. Preheating to the austenitising temperature should be done gradually to prevent excessive temperature differences. The first stage should be between 590 and 680 ºC until

the temperature between the centre and surface is lower than 110 ºC. The second stage should occur between 815 and 860 ºC and continue until temperatures are compensated with a difference no greater than 14 ºC. The austenitisation temperature should be reached with a holding time of 30 minutes after temperature compensation or for a maximum of 90 minutes until the austenitisation temperature is obtained on the surface. Quenching should be carried out at a minimum rate of 28 ºC/min. For large dies with cross sections above 30 mm, interrupted quenching at a surface temperature of 400 to 450 ºC should be applied when the centre temperature diverges by more than 110 ºC. After quenching, tempering should be performed, and the work-pieces should not be cooled below 33 ºC. The initial tempering process is conducted at a minimum temperature of 565 ºC and held for a duration dependent on the tool's cross section, with a minimum of 2 hours. Following this, the tool is cooled to ambient temperature before undergoing a second tempering process at a minimum temperature of 550 ºC. A third tempering process may be applied for hardness adjustment, although it is not mandatory. Typically, the desired hardness falls between 42 and 52 HRC. These requirements can be achieved in a single-chamber vacuum furnace equipped with a high-pressure cooling system in an inert gas. A vacuum furnace allows for the entire process to be completed in a single piece of equipment without transferring the workload, in a single work cycle [21, 29].

Chapter 3

Experimental Procedure

This chapter focuses on the experimental procedure used to study the influence of heat treatment cycle parameters on the microstructure and mechanical properties of AISI H11 Premium steel. It includes sections related to the material, heat treatment cycles, methodologies for microstructural characterisation, and mechanical testing, specifically hardness, and absorbed energy tests.

3.1 Material

AISI H11 Premium is a medium-carbon, high-alloy hot work tool steel that belongs to the grade of chromium hot work tool steels [2]. These grade of steel is part of the new generation of modified H11 (1.2343) steel grades with a low silicon content [18]. A metalworking industry provided a 500 x 500 x 20 mm plate of AISI H11 Premium, from the original 600 x 500 x 500 mm forged plate, for this study to produce specimens for microstructural characterisation, hardness, and impact tests and for dilatometry studies. All specimens were taken from the centre of the plate. The chemical composition of AISI H11 Premium is presented in Table 3.1 [10, 11].

Table 3.1: Chemical composition (wt. %) of the AISI H11 Premium.

Element	C	Si	Mn	P	S	Cr	Mo	V	Fe
AISI H11 Premium	0.32 - 0.42	0.10 - 0.40	0.20 - 0.40	0.030	0.003	4.80 - 5.50	1.10 - 1.40	0.30 - 0.60	Bal.

AISI H11 Premium is known for its high toughness and shock resistance [2]. To meet the demands of high temperature impact loading, softening during high temperature exposure, and thermal

fatigue, this grade of chromium hot work tool steels requires medium carbon contents and relatively high concentrations of chromium and other strong carbide-forming elements [9]. Heat treatment parameters are traditionally selected based on the desired final hardness for a specific application. It is important to correlate these mechanical properties with the material's tensile behaviour, as shown in Table 3.2. Table 3.3 displays the thermal and physical properties of this steel, along with its impact energy at room temperature [9, 18]. These values are related to quenched and tempered specimens.

Table 3.2: Hardness' influence on AISI H11 Premium tensile behaviour [18].

Hardness (HRC)	**Tensile Strength (MPa)**	**Yield Strength (MPa)**	**Elongation (%)**
45	1450	1240	13
47	1580	1340	13
49	1680	1410	12

Table 3.3: AISI H11 Premium properties [18].

Density (kg/m^3)	**Coefficient of Thermal Expansion (10^{-6} m/mK)**	**Thermal Conductivity (W/m°C)**	**Impact Energy (T_{amb}) (J)**
7.800	11.6 - 13.20	30 - 31	30

3.2 Heat Treatment Cycles

This section outlines the parameters selected for the heat treatment cycles. The austenitisation and quenching heat treatment were performed, followed by a triple tempering and conditions corresponding to the centre and surface of a large mould (around 500 kg). This recommendation was made by the company responsible for overseeing this particular project. It is evident that the surface of the tool reaches the temperature of the furnace at a considerably faster rate (12 ºC/min) than the centre (2 ºC/min), which results in a thermal gradient. This phenomenon results in a longer period of austenitisation for the surface in comparison with the centre, as depicted in Figure 3.1 (a) and (b) [17]. The holding time for the surface was calculated based on the time required for the centre to reach the preset temperature.

In order to define the parameters, dilatometry tests were performed to ascertain the phase transformations of the AISI H11 Premium steel when heating rates of 2 ºC/min and 12 ºC/min were to be employed. It can be concluded that when heating at a rate of 12 ºC/min, the initial temperature of austenitisation, A_{c1}, commenced at 820 ºC and the conclusion of austenitisation, A_{c3}, was reached at 920 ºC (Figure 3.2). Conversely, a heating rate of 2 ºC/min resulted in an initial austenitisation

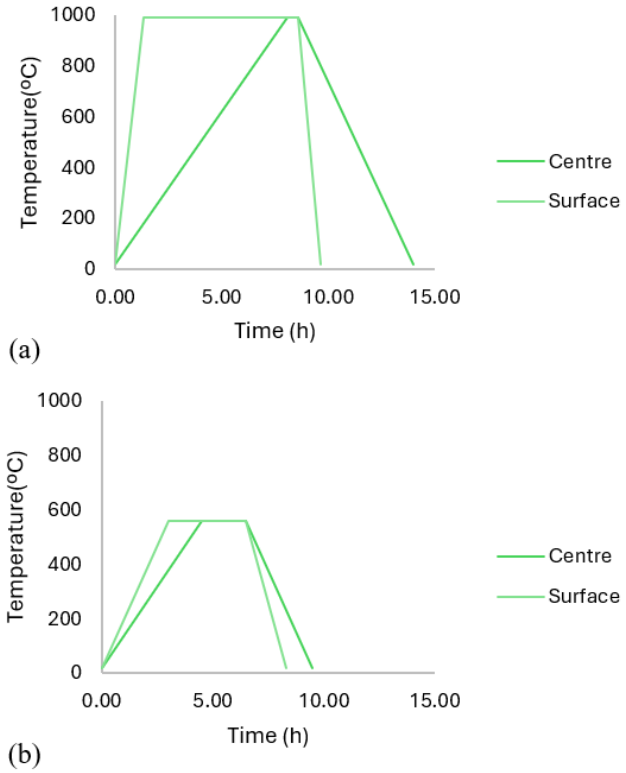

Figure 3.1: Representation of the thermal gradient observed between the surface (12 ºC/min) and that of the centre (2 ºC/min) for (a) austenitisation and quenching and (b) tempering.

temperature of 800 ºC and an end point of 880 ºC (Figure 3.3). Indeed, the phenomenon of thermal hysteresis can be invoked to explain the observation that when a higher heating rate is employed (12 ºC/min), the austenitic transformation will commence and conclude at temperatures that are higher than those observed when a lower heating rate is used (2 ºC/min).

Furthermore, it was determined that when a heating rate of 12 ºC/min is applied, a holding time of 30 minutes is set, and the material is cooled at 50 ºC/s, the martensite transformation commences, reaching M_s at 360 ºC and concluding with M_f at 80 ºC. It is crucial to highlight that the initiation and conclusion of the martensite transformation are contingent upon the holding time, yet remain unaffected by the cooling rate.

We defined a austenitisation temperature of 990 ºC. A review of the literature indicates that this value is situated within the lower range of austenitisation temperatures for AISI H11 Premium [2, 5, 6, 8, 14, 18, 23, 24, 30, 31]. It was determined that the A_{c3} temperature is 920 ºC when a heating rate of 12 ºC/min is applied. It is typically recommended that the temperature exceed 50°C to ensure that the heat treatment is performed within the austenitic domain. Furthermore, it was observed that the set temperature (990 ºC) is 70 ºC higher than this value, and could potentially be reduced to

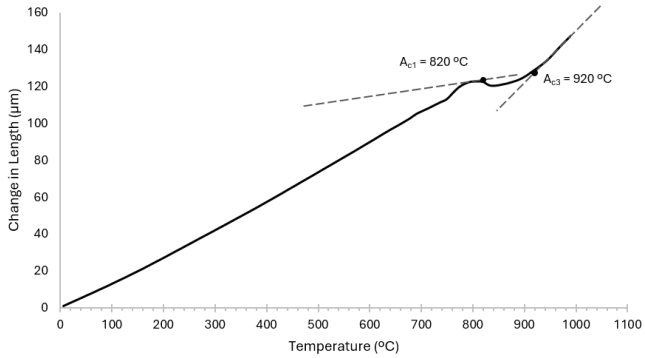

Figure 3.2: Determination of transition temperatures A_{c1} and A_{c3} with continuous heating at 12 ºC/min.

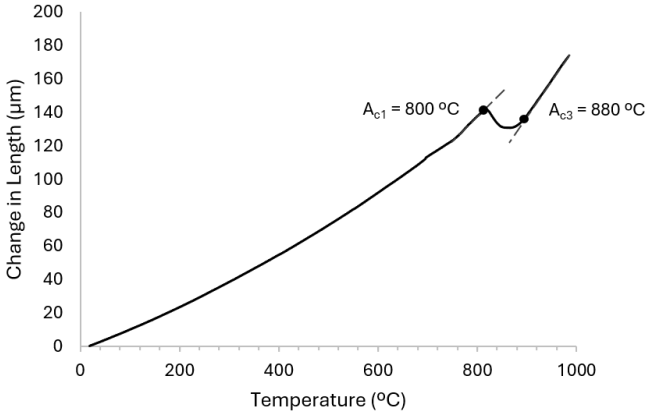

Figure 3.3: Determination of transition temperatures A_{c1} and A_{c3} with continuous heating at 2 ºC/min.

970 ºC. However, the parameters were set based on industrial experience, and 990 ºC is typically employed for the austenitisation of the AISI H11 Premium steel. Indeed, it is inadvisable to exceed the austenitisation temperature, as this can result in a significant increase in grain growth, which in turn leads to a reduction in the strength of the material and a subsequent decrease in tool life [7]. As a general rule, holding times are typically between 30 and 45 minutes. However, as previously stated, due to the dimensions of the components, a thermal gradient is observed between the surface and the centre of the tool. This results in the surface undergoing longer holding times than the centre. In order to avoid excessive grain growth, a value of 30 minutes has been set on the lower end of the range [5, 8, 18, 30, 31]. In this context, a holding time of 30 minutes for the centre of the tool will result in a considerably longer surface exposure time, ranging from 424 to 434 minutes, contingent on the ΔT applied. In light of the findings of our research, we have determined that the optimal tempering temperature is 560 ºC. Furthermore, we have established that a two-hour tempering time is

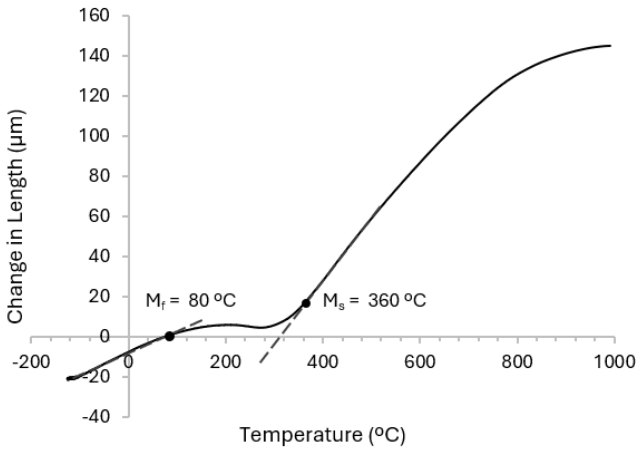

Figure 3.4: Determination of transition temperatures M_s and M_f with a holding time of 30 minutes and continuous cooling at 50 ºC/s.

optimal [2, 6, 8, 14, 18, 23, 24, 30, 31, 32]. A triple tempering process was conducted with identical parameters. It is imperative to double temper this type of steel, and triple tempering is recommended for enhanced performance [33]. The heating rate values, as presented in Tables 3.4 and 3.5, represent the typical heating rate values observed for large-dimension moulds in the heat treatment industry. The furnaces utilised for tempering have a lower power rating than those employed for austenitisation heat treatment, resulting in a notable reduction in the heating rate. The specimens were cooled in an air medium in both the quenching and tempering processes. All parameters were defined in accordance with the specifications set forth by the company involved in the project, with due consideration given to the industrial experience acquired by the company.

The parameters for the austenitisation process can be observed in Table 3.4, in which C1-C9 represent the conditions corresponding to the behaviour of the centre of the tool (Figure 3.5), and S1-S9 (Figure 3.6) correspond to the behaviour of the surface of the tool. Furthermore, the S10 parameter set represents the absence of a thermal gradient, which would be observed in a component of small dimensions. It is presented here for comparison with the behaviour observed in large moulds (Figure 3.7). In the table, $t_{\Delta T}$ corresponds to the time interval between the initial set temperature and the final set temperature, with the temperature difference represented by the parameter ΔT. On the other hand, $t_{990ºC}$ is the time spent at the set temperature (990 ºC).

In addition, the parameters for the tempering process are delineated in Table 3.5. These parameters pertain to the three tempering cycles that were conducted. It is crucial to highlight that the conditions subjected to tempering were selected based on the results of the austenitisation and quenching conditions. In particular, the selection was based on the hardness, retained austenite, and grain size. Only

Table 3.4: Austenitisation conditions and parameters.

Condition ID	**Heating Rate (ºC/min)**	**T (ºC)**	**ΔT (ºC)**	**$t_{\Delta T}$ (min)**	**$t_{990ºC}$ (min)**
C1 - C3	2	990	N/A	N/A	30
C4 - C6			10	5	25
C7 - C9			20	10	20
S1 - S3	12		N/A	N/A	435
S4 - S6			10	5	430
S7 - S9			20	10	425
S10			N/A	N/A	30

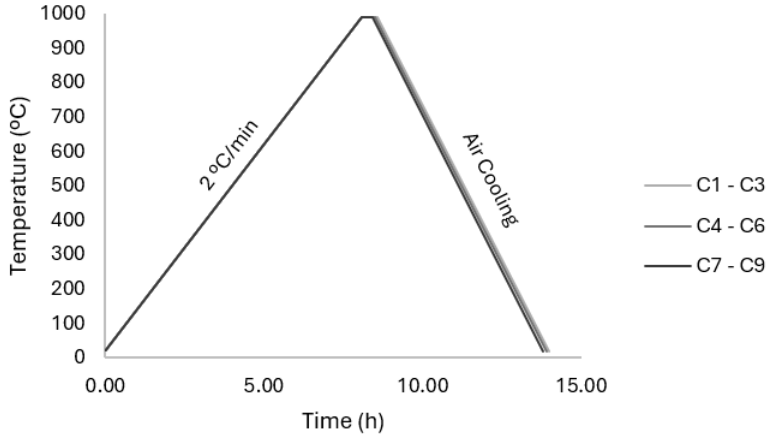

Figure 3.5: Austenitisation and quenching cycles corresponding to the centre of the tool.

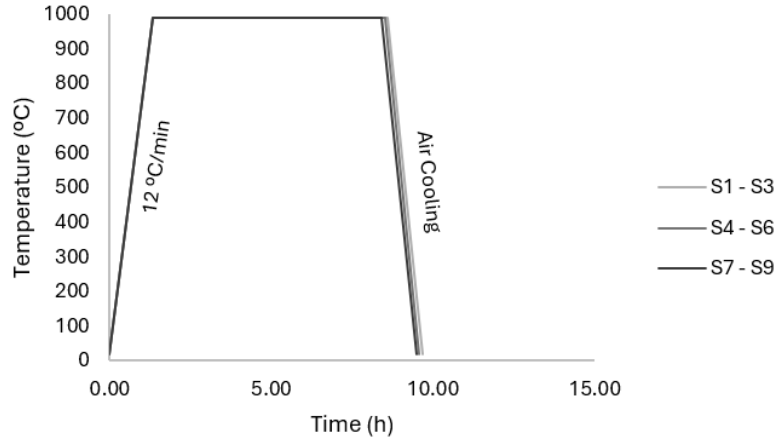

Figure 3.6: Austenitisation and quenching cycles corresponding to the surface of the tool.

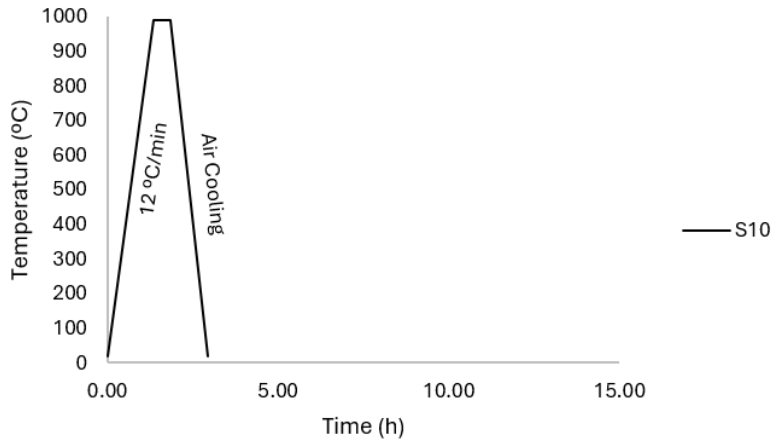

Figure 3.7: Austenitisation and quenching cycles corresponding to the S10 condition.

those who could demonstrate the most favourable results in terms of mechanical and microstructure properties, as well as heat treatment time optimisation, were selected for further tempering. The tempering cycles are presented in Figures 3.8, 3.9 and 3.10, for the conditions of the centre, of the surface and when no thermal gradient is observed, respectively. Similarly, as previously outlined for the quenching conditions, $t_{\Delta T}$ corresponds to the time interval between the initial set temperature and the final set temperature, with the temperature difference represented by the parameter ΔT. On the other hand, $t_{560ºC}$ is the time spent at the set temperature (560 ºC).

Table 3.5: Tempering conditions and parameters.

Condition ID	**Heating Rate (ºC/min)**	**T (ºC)**	**ΔT (ºC)**	**$t_{\Delta T}$ (min)**	**$t_{560ºC}$ (min)**
C7	2	560	N/A	N/A	120
C8			10	40	80
C9			20		
S7	3		N/A	N/A	210
S8			10	128	82
S9			20	127	83
S10			N/A	N/A	120

3.3 Microstructural Characterisation

The microstructural characterisation of the AISI H11 Premium involved the preparation of metallographic samples, followed by optical and electron microscopy of the as-received and heat-treated

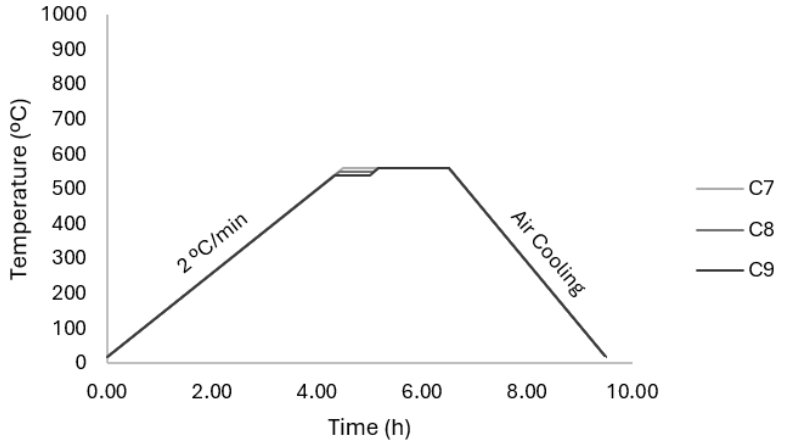

Figure 3.8: Tempering cycles corresponding to the centre of the tool.

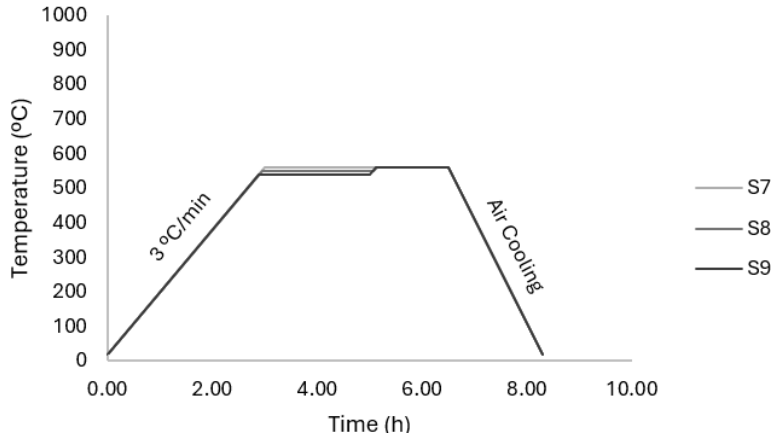

Figure 3.9: Tempering cycles corresponding to the surface of the tool.

samples. Furthermore, carbide extraction was conducted on the as-received sample. A XRD analysis was conducted on the extracted carbides, to assess their stoichiometry, as well as on the quenched samples, to measure the amount of retained austenite.

Figure 3.11 illustrates the methodology employed for the retrieval of samples from the plate. The outer dashed lines are indicative of the original plate (600 x 500 x 500 mm) and the light grey areas represent the supplied plate (500 x 500 x 20 mm). The inner dashed lines (100 mm) correspond to the material removed from the surface of the plate, thus allowing for a detailed analysis of the central region, which was obtained by means of plasma cutting. In order to cut into smaller sections, an Optimum S275N saw, manufactured by Optimum Machinen Germany GmbH, and a PRESI Mecatome abrasive disk were employed. As it can be observed, tensile and Charpy-V Notch Impact Test (CVN) specimens were extracted from the plate and subsequently machined in accordance with the most

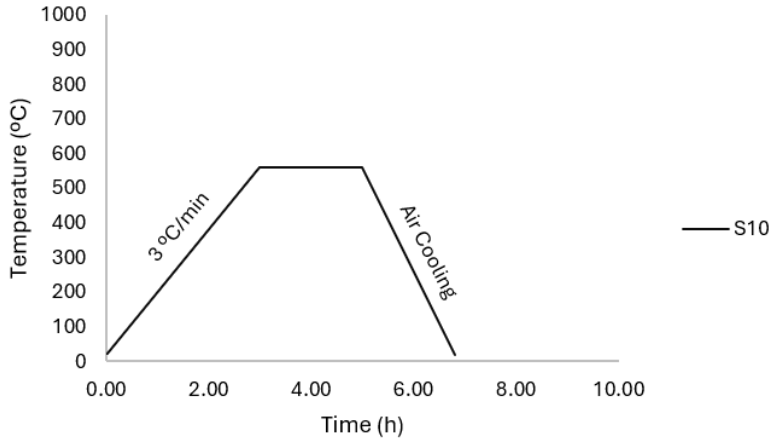

Figure 3.10: Tempering cycle corresponding to the S10 condition.

unfavourable direction. The samples for microstructural characterisation were obtained from the remaining plate material following the removal of the requisite material for the tensile and impact tests. A total of 80 samples, each measuring 10 x 10 x 10 mm, were obtained.

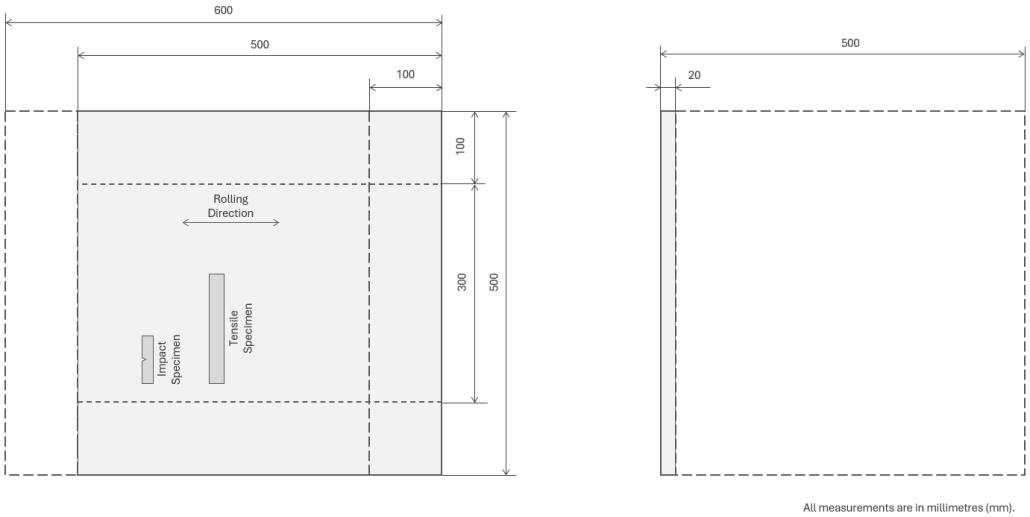

Figure 3.11: Representation of the methodology employed to retrieve the samples from the plate.

Metallographic preparation involved a P120-4000 grit silicon carbide sandpaper sequence, followed by a polishing step with a 1 µm diamond suspension and the respective cloth. The chemical etching was conducted using a 2 % Nital solution for the annealed structure and the Villela's reagent to reveal the microstructure of the quenched and tempered samples [34, 35]. The following chemical and electrolytic etchants were used in an unsuccessful attempt to reveal the prior-austenite grain size:

- Chemical etching with a solution of 80 mL ethanol, 10 mL nitric acid, 10 mL hydrochloric acid and 1 g picric acid for 5 to 10 minutes;
- Electrolytic etching with a solution of 20% NaOH, for 5 to 10 seconds, at a voltage of 6 V;
- Electrolytic etching with a solution of 40% NaOH, for 5 to 10 seconds, at a voltage of 6 V;
- Electrolytic etching with a solution of 60% HNO_3, for 120 seconds, at a voltage of 1 V [34].

The Optical Microscopy (OM) micrographs were obtained using a Leica DM4000 M microscope with a DMC 2900 camera. In contrast, the OM micrographs of the grain size were obtained using a Leica DVM6 digital microscope with a PLANAPO FOV 3.6 objective and the multifocus tool, as the faces were not flat and level. A Scanning Electron Microscopy (SEM) analysis was conducted using the Phenom^{TM} XL G2 Desktop SEM. The XRD measurements were carried out in a Bruker D8 Discover diffractometer, with step size of 0.02º, time per step 1 s and 2θ angular interval of 20 - 80º. A CuK_α (1.54060 Å) beam was used at 40 kV and 40 mA. The volume fractions of the austenite (γ) and martensite (α) phases were obtained by the direct comparison method using the following equations:

$$\frac{I_\alpha}{I_\gamma} = \frac{K_\alpha C_\alpha}{K_\gamma C_\gamma} \tag{3.1}$$

$$K_{\alpha,\gamma} = \frac{1}{v^2}\left(|F|^2 m\left(\frac{1+cos^2\theta}{sin^2\theta cos\theta}\right)\right)\left(\frac{e^{-2M}}{2\mu}\right) \tag{3.2}$$

$$C_\alpha + C_\gamma = 1 \tag{3.3}$$

where v is the unit cell volume of each phase, F is the structure factor, m is the multiplicity factor, θ is the reflection angle of the analysed peak, e^{-2M} is the Debye-Waller factor and μ is absorption coefficient of each phase. The diffraction peaks were selected on the basis of the four-peak method (two peaks of martensite and two peaks of austenite) and compared all against all. The average value of all compared diffraction peaks was calculated to minimise the effect of the preferred direction. The peaks under consideration were $(111)_A$ and $(200)_A$ for austenite and $(110)_M$ and $(200)_M$ for martensite [36, 37, 38, 39]. The prior austenite grain size was determined through the implementation of a thermal etching cycle, as illustrated in Figure 3.12, utilising the alpha measuring system of a TA

Instruments DIL805 dilatometer. The dilatometry specimens were 4 mm in diameter and 10 mm in length, previously quenched according to the conditions previously presented, and followed the metallographic preparation presented in Section 3.3, with the exception of the chemical etching. Prior to the test, the metallographic preparation is conducted on the specimen's sides. Following the test, the samples were subjected to a brief polishing process with a 1 µm diamond suspension and the corresponding cloth for approximately 30 seconds. This was done to remove the oxidation layer, after which direct observation was conducted using light microscopy, as previously mentioned.

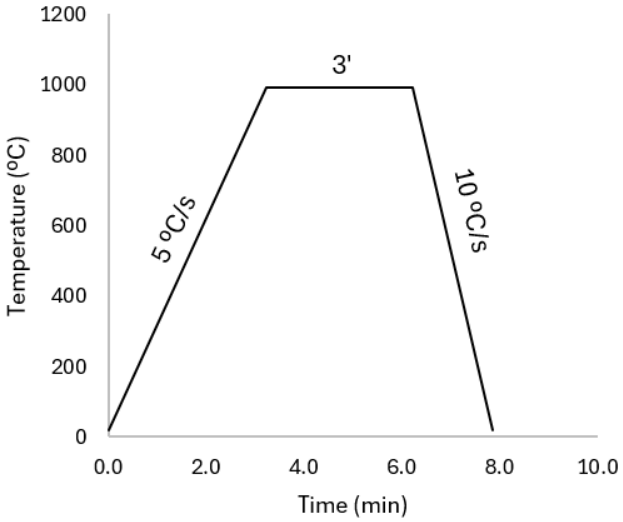

Figure 3.12: Thermal etching cylce.

The prior-austenite grain size was ascertained through the utilisation of the ImageJ application. A total of 100 grains were measured in at least five different fields, with the area of each grain subsequently calculated. In order to determine the grain size, it was assumed that the grain in question exhibited a hexagonal shape. In order to ascertain the ASTM E112 grain size (G), the ASTM E112 standard was consulted [40]. It should be noted that the conditions S1 and S4 were not subjected to investigation, as it was determined that the discrepancy in holding time between these and S7 would not impact the grain size.

The process of carbide extraction was conducted on the as-received annealed sample. The precipitates were extracted by dissolution of the matrix using the Berzelius reagent (1.85 L distilled water, 320 g cupric chloride, 280 g potassium chloride, 150 mL hydrochoric acid and 20 g tartaric acid) and the Nital 10% reagent (10 mL nitric acid and 90 mL ethanol). A total of four samples were dissolved, with two samples dissolved in each solution. Approximately 0.7 g of the each sample was dissolved in 50 mL of Nital 10% and 75 mL of the Berzelius solution. The resulting solution was then vacuum

filtered through a 0.2 µm pore size filter, with both the filter and the precipitates being washed with distilled water and subsequently dried at 100 °C, for two hours [41, 42].

3.4 Mechanical Characterisation

The mechanical characterisation delineates the macroscopic methodologies utilized for the analysis of the mechanical properties of the AISI H11 Premium steel. These include hardness and impact testing.

A total of six Rockwell C hardness tests were conducted on each quenched ant tempered specimen using a universal hardness tester, specifically the Dura Vision 20 manufactured by EMCO-TEST Prüfmaschinen GmbH. The tests were conducted using an indentation apparatus, with an indentation time of 10 seconds. Furthermore, a total of six Brinnel hardness tests were conducted on the as-received sample using a load of 5/250. A Charpy Pendulum HOYTOM 300J AD2 was employed to perform a CVN in accordance with the standard NP EN ISO 148-1:2016, at room temperature, more specifically, 23 ºC. The dimensions of the specimens subjected to testing are presented in Figure 3.13 [43]. A total of two specimens were tested for each condition.

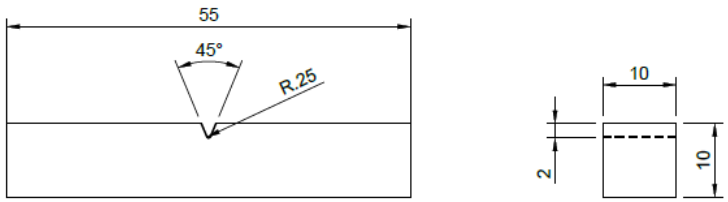

Figure 3.13: Dimensions of the impact test specimen, according to NP EN ISO 148-1:2016.

Chapter 4

Results and Discussion

This chapter presents the findings of the research project and a critical analysis of the findings of the conducted research. The initial section is dedicated to the commercialised state, which is the annealed condition, encompassing microstructure, extracted carbides and hardness. Subsequently, the second and third sections of the chapter are devoted to the microstructural and mechanical characterisation of the quenched and tempered samples of AISI H11 Premium steel, with a particular focus on the correlation between mechanical characterisation and microstructure analysis.

4.1 Annealed Condition

The microstructure of the AISI H11 Premium steel in its as-received state is comprised of an annealed microstructure, which is characterised by a ferritic matrix and a distribution of globular carbides. This is illustrated in Figure 4.1. The carbides present are more complex than cementite, given the high alloy content of the steel. The results of the SEM coupled with Energy-Dispersive X-ray Spectroscopy (EDS) analysis of the annealed sample demonstrated the presence of iron-molybdenum, iron-vanadium and iron carbides, as illustrated in Figure 4.2. It is possible that the annealed SEM analysis may yield results indicating the presence of M_2C, MC and M_3C, respectively. However, it should be noted that the SEM/EDS analysis is semi-quantitative in nature, and therefore, it is not possible to draw definitive conclusions regarding the stoichiometry of the carbide. The sample in its as received state exhibited a hardness of 160 HBW $\pm$ 2 HBW.

Moreover, the extracted carbides from the annealed sample were subjected to examination under SEM/EDS, which revealed that their primary composition consisted of vanadium (V) and iron-chromium (Fe-Cr). The aforementioned analysis permitted the conclusion to be drawn that the carbides exhibit a spherical morphology, as demonstrated in Figure 4.3 (a) and (b). XRD analysis of the powder extracted from the annealed sample revealed the presence of $M_{23}C_6$ (M: predominantly

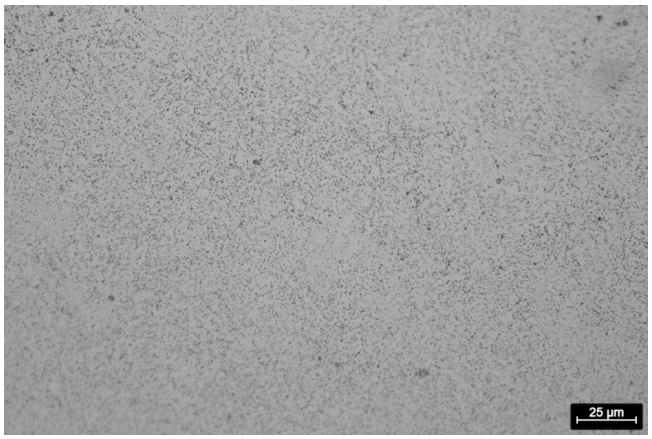

Figure 4.1: OM micrograph of the annealed AISI H11 Premium steel revealing a ferritic matrix and a dispersion of primary carbides.

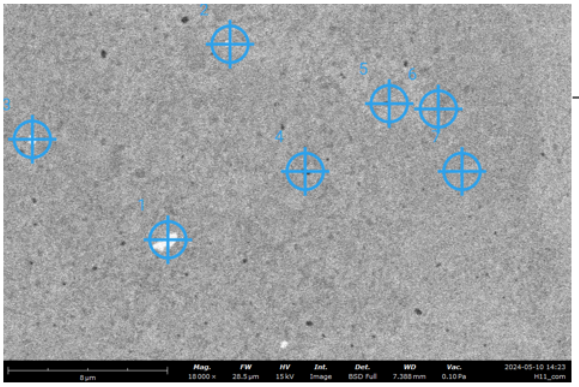

Spot	Elements Weight Concentration (%)					Possible Carbide Type
	C	V	Cr	Fe	Mo	
1	23.6	1.3	4	42.6	26.8	M_2C
2	22.9	0.9	6.5	55.4	13.6	M_2C
3	23.1	1.0	3.5	52.2	17.7	M_2C
4	23.2	15.1	5.2	52.7	3.8	MC
5	22.1	12.9	5.6	55.7	3.7	MC
6	21.2	0.8	6.4	70.2	1.4	M_3C
7	20.2	0.6	4.4	74.7	-	M_3C

Figure 4.2: SEMEDS micrograph of the annealed AISI H11 Premium steel and the respective determination of possible carbide types.

Fe and Cr) and M_3C (M: predominantly Fe) carbides, as shown in Figure 4.4 (a) from the Berzelius reagent and Figure 4.4 (b) from a 10% Nital solution.

The annealing process results in the transformation of austenite into ferrite and the formation of additional spheroidised carbides upon cooling, a phenomenon that was indeed observed. Tool steels are commercialised in the annealed state, facilitating their subsequent mechanical processing to achieve the desired final geometry of the part. Furthermore, the present carbides are more complex than cementite, as evidenced by the SEM/EDS analysis, which identified the presence of V, Fe-Cr, Fe-Mo and Fe carbides. Additionally, the XRD analysis confirmed the existence of $M_{23}C_6$ and M_3C, thereby corroborating the aforementioned findings. As indicated in the literature, and mentioned in the Subsection 2.2.3, the annealed microstructure should be characterised by the presence of M_2C,

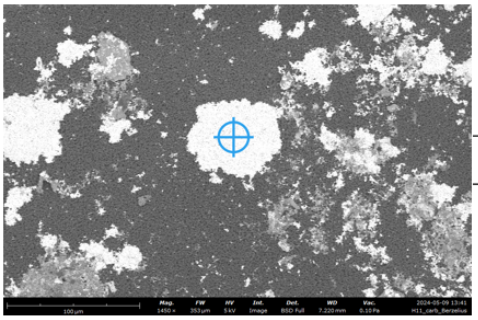

(a)

Elements Weight Concentration (%)					Possible Carbide Type
C	V	Cr	Fe	Mo	
11.8	43.0	22.8	13.4	9.0	MC

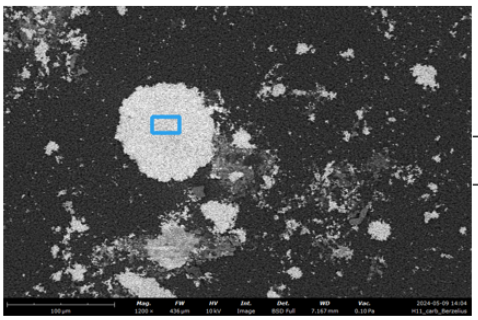

(b)

Elements Weight Concentration (%)					Possible Carbide Type
C	V	Cr	Fe	Mo	
5.9	8.2	32.7	39.0	7.3	$M_{23}C_6$

Figure 4.3: SEM/EDS micrograph of the (a) V-Fe carbide and (b) Cr-Fe carbide.

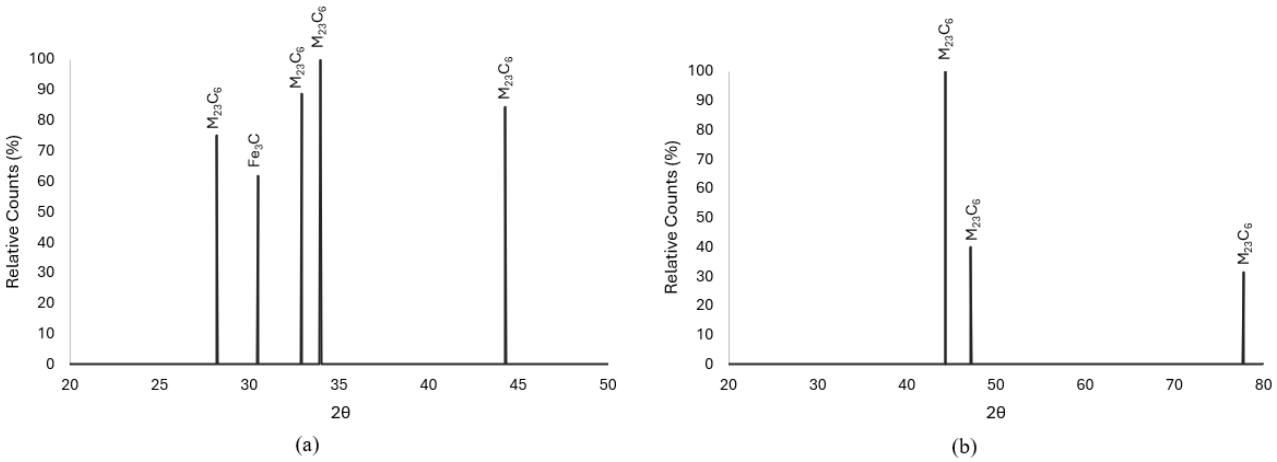

Figure 4.4: Carbide identification of the carbides extracted from the annealed sample using (a) the Berzelius reagent and (b) a 10% Nital solution.

M_3C, $M_{23}C_6$ and small quantities of MC. However, the analysis did not identify these fully. It is plausible that during the extraction process, some of the elements were dissolved, or that the filtration apparatus employed was not sufficiently small to retain the smaller carbides [26, 44, 45, 46, 47]. In accordance with the specifications set forth by the NADCA, the annealed microstructure exhibits a

hardness value that falls below 250 HB, with a precise measurement of 160 HB.

4.2 Quenched Conditions

The nomenclature of the samples is in accordance with the conditions identified in Table 3.4 of Section 3.2. Figure 4.5 depicts the OM micrographs of the (a) central region of the tool (C1) and (b) surface of the tool (S1) following the application of the conventional austenitisation and quenching process, wherein the ΔT = 0 ºC. The SEM micrographs of the centre and surface of the tool can be found in Figure 4.5 (c) and (d), respectively.

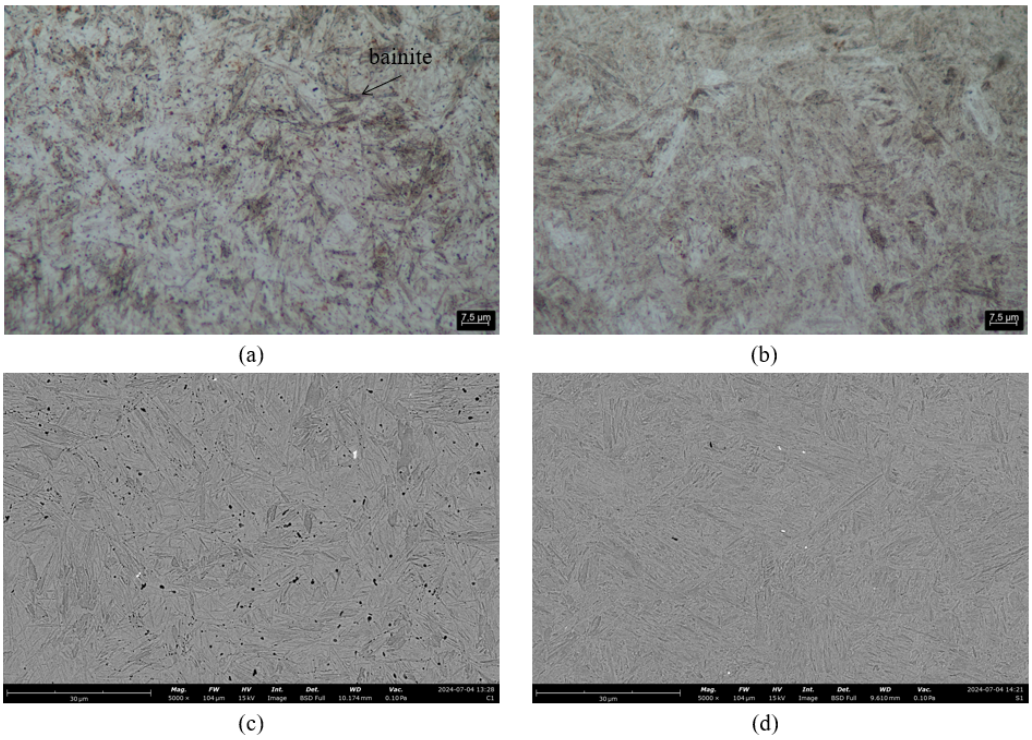

Figure 4.5: OM micrographs of (a) C1, with a holding time of 30 minutes and (b) S1, with a holding time of 435 minutes, representing a martensitic matrix with a minor dispersion of carbides and SEM micrographs of quenched microstructure of the (c) centre (C1) and (d) surface (S1) of the tool

Figure 4.6 outlines the OM micrographs of the centre (C4) and surface (S4) of the tool when a ΔT of 10 ºC is applied during the austenitisation process. Figure 4.6 (c) and (d) represents the SEM images of the C4 and S4 regions, respectively.

Figure 4.7 depicts the OM micrographs of the tool's centre (C7) and surface (S7) when a ΔT of 20 ºC was applied during austenitisation. Furthermore, the SEM images of C7 and S7 are presented in Figure 4.7 (c) and (d), respectively.

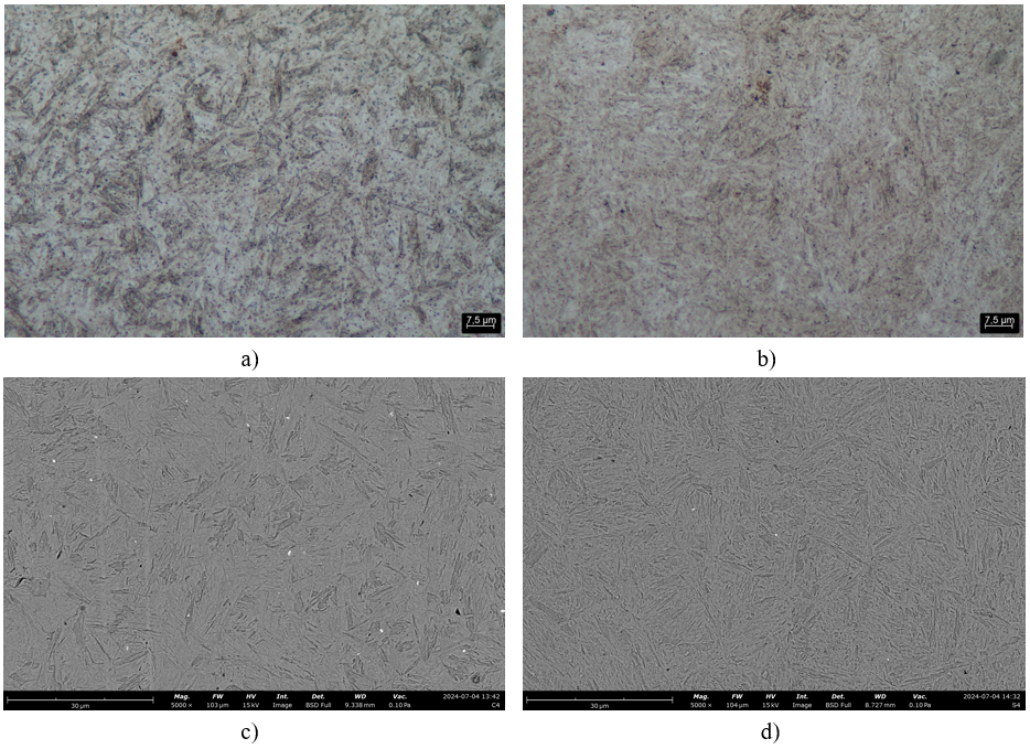

Figure 4.6: OM micrographs of quenched microstructure of the (a) centre (C4), with a holding time 25 minutes and (b) surface (S4) of the tool, with a holding time of 430 minutes, representing a martensitic matrix with a minor dispersion of carbides and SEM micrographs of (c) C4 and (d) S4.

Figure 4.8 illustrates the microstructure of the material when there are no thermal gradients, resulting in the formation of a martensitic matrix. This is demonstrated in Figure 4.8 (a) and (b), which present the results of OM and SEM analysis, respectively. The carbide dispersion is composed of iron carbides, which were identified using SEM coupled with EDS.

The microstructure of the quenched samples is constituted by a martensitic matrix and a minor dispersion of carbides, detected by SEM coupled with EDS. All conditions related to the centre presented iron and iron-molybdenum carbides, whereas the surface conditions exhibited iron carbides, which are believed to be cementite. It is plausible that precipitation occurred during the quenching process, and that other carbides may be present; however, only these were detected. The presence of molybdenum carbides may be attributed to an insufficient period of time for dissolution. It is crucial to acknowledge that each carbide exhibits a distinct dissolution interval. Martensite can manifest in a multitude of structural forms; in the present case, it is postulated to be lath martensite. Nevertheless, additional characterisation is required to ascertain its morphology. The formation of bainite is a typical consequence of air cooling employed subsequent to austenitisation.

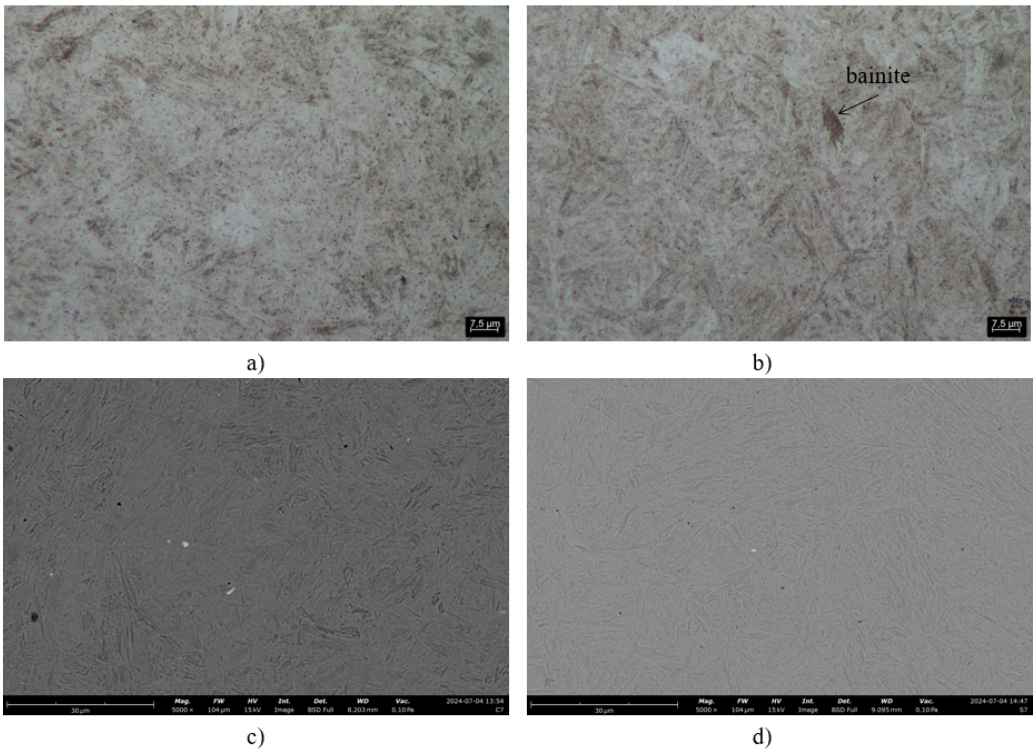

Figure 4.7: OM micrographs of quenched microstructure of the (a) centre (C7), with a holding time of 20 minutes and (b) surface (S7) of the tool, with a holding time of 425 minutes, representing a martensitic matrix with a minor dispersion of carbides and SEM micrographs of (c) C7 and (d) S7.

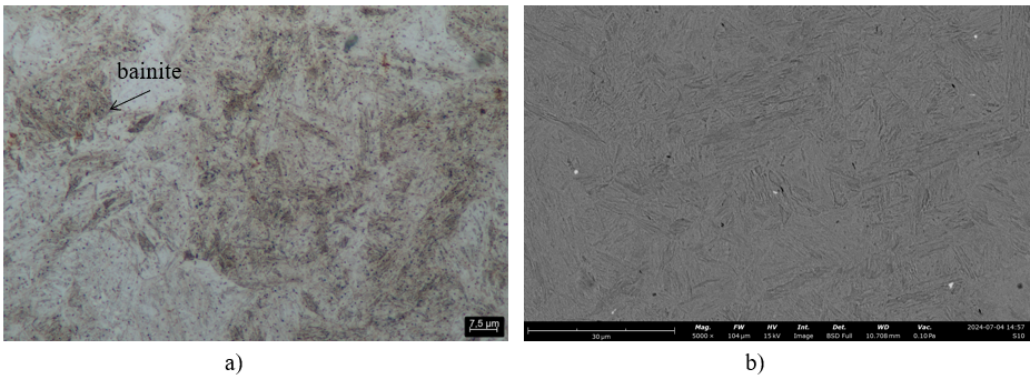

Figure 4.8: (a) OM micrograph of the condition corresponding to the S10, when no thermal gradients are considered, with a holding time of 30 minutes, representing a martensitic matrix with a minor dispersion of carbides and (b) its SEM micrograph.

The final structure, resulting from the combination of austenitisation and air cooling, is characterised by the presence of a martensitic microstructure, with traces of bainite and residual austenite, as

well as a minor fraction of undissolved carbides. This observation was consistently evident across the entire range of austenitising and quenching conditions. Martensite can manifest in a variety of morphologies. In tool steels with a chromium content exceeding 1 wt.%, $\{225_f\}$ plates can be observed, in addition to lath martensite. Nevertheless, the aforementioned structures cannot be identified through OM or SEM. Therefore, a more sophisticated characterisation technique, such as TEM, is necessary [32, 48, 49, 50, 51]. Furthermore, it can be hypothesised that the darker regions, presented in Figures 4.5, 4.6 and 4.8 in the microstructure may be attributed to the presence of bainite, which is a typical occurrence when air cooling is employed following quenching [52]. Finally, the presence of residual austenite is anticipated, although it can only be discerned in OM for percentages exceeding 15% [53].

Although the literature indicates that carbides of the types MC, $M_{23}C_6$ and M_3C can be found after quenching, the SEM/EDS analysis was only able to identify carbides containing iron and iron-molybdenum, which could correspond to the stoichiometry of the M_3C and M_2C carbide types, respectively [25, 54]. A review of the literature reveals that the formation of molybdenum carbides can occur as a result of their precipitation upon cooling at a low rate [54]. Nevertheless, such a conclusion can only be reached through the utilisation of techniques such as XRD or TEM. The absence of carbides of the MC and $M_{23}C_6$ types may be attributed to their nanometric size, which is not discernible with the SEM magnification [25, 55]. The Fe-Mo carbides were identified as a significant factor in the conditions related to the centre of the tool, which account for a lower holding time, approximately 15 times shorter than that observed at the surface. This indicates that the time for carbide dissolution was limited. This also provides a rationale for the qualitative conclusion that the centre exhibits a higher carbide volume.

Figure 4.9 demonstrates a correlation between hardness and retained austenite with holding time. The centre of the tool exhibited hardness values of 54 HRC $\pm$ 3 for, 53 HRC $\pm$ 2 and 53 HRC $\pm$ 1 HRC for C1, C4 and C7, respectively. In contrast, the surface of the tool demonstrated hardness values of 47 HRC $\pm$ 2, 47 HRC $\pm$ 1, and 46 HRC $\pm$ 1 HRC for S1, S4, and S7, respectively. Furthermore, the condition that did not take into account thermal gradients (S10) exhibited a hardness of 51 HRC $\pm$ 1 HRC. In contrast, retained austenite exhibited minimal variation across the various holding times, with values ranging between 4.2% and 5.2%. The exception was the 2.5% sample C4. The data retrieved from the XRD analysis can be found in B.

It is anticipated that the AISI H11 Premium tool steel will attain hardness values of between 53 and 55 HRC following quenching [56]. This was demonstrated in the samples that were held for a period of 30 minutes or less. However, the hardness values observed for the surface conditions fell between 46 and 47 HRC. A review of the literature indicates that values of 1.8 to 2.5 % of retained austenite can be detected after quenching. However, these values are located at the lower end of the XRD detection limits, which may result in a lack of precision in the detection process [57].

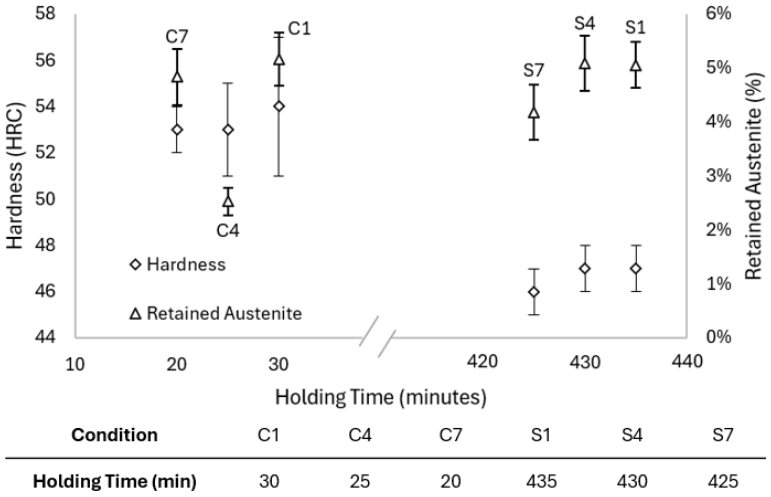

Condition	C1	C4	C7	S1	S4	S7
Holding Time (min)	30	25	20	435	430	425

Figure 4.9: Hardness (HRC) and retained austenite (%) versus holding time of the quenched samples.

Despite the expectation of an increase in the amount of retained austenite for surface conditions due to the longer holding time and consequently higher austenite stabilisation, this was not significantly observed. It can be posited that, in the present case, the duration of the holding time is not a factor influencing the volume fraction of residual austenite. However, potential errors in the determination of the amount of residual austenite in each sample could be the reason behind the non-significant difference observed between the centre and surface conditions. The aforementioned errors may be attributed to an erroneous detection of the XRD peaks or to approximations in the values employed for the calculation. It is evident that a considerable prolongation of the austenitisation period will have a marked impact on the material properties. An increase in austenitisation time allows for a greater dissolution of carbides and more effective stabilisation of austenite, which can result in a reduction in hardness [17, 58]. However, as previously stated, the results for the retained austenite did not exhibit a notable discrepancy between the centre and surface conditions, indicating that this cannot be the primary factor responsible for the observed decrease in hardness.

Figure 4.10 illustrates the impact of varying holding time on the variation of hardness and grain size. The central region of the tool displays grain sizes of approximately 20 μm $\pm$ 5 μm, 21 μm $\pm$ 4 μm and 24 μm $\pm$ 5 μm for holding times of 30 (C1), 25 (C4) and 20 (C7) minutes. In contrast, the surface presents a grain size of 35 μm $\pm$ 8 μm for a holding time of 425 minutes (S7). In accordance with the ASTM E112 standard, the central region of the tool exhibits a grain size (G) of 8.5, while the surface displays a value of 7. Ultimately, in the absence of a thermal gradient, a grain size of 23 μm $\pm$ 6 μm would be attained, corresponding to a grade of 8.5 in accordance with the ASTM E112 standard.

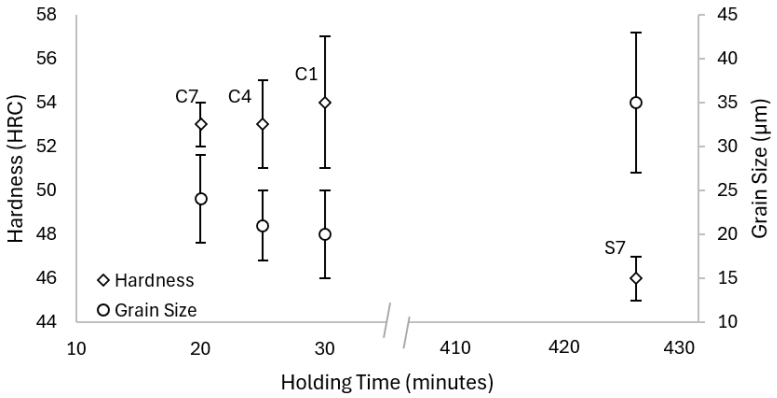

Figure 4.10: Hardness (HRC) and grain size (μm) versus holding time of the quenched samples.

The OM micrographs corresponding to the grain size of the condition that allows the lowest holding time are presented in Figure 4.11. Figure 4.11, panel (a) depicts the centre of the tool, with a holding time of 20 minutes (C7), while panel (b) shows the surface of the tool, with a holding time of 425 minutes (S7). Through a detailed analysis using ImageJ and subsequent calculations, we can conclude that the surface condition exhibits a grain size that is approximately 1.5 times larger than that observed in the centre of the tool.

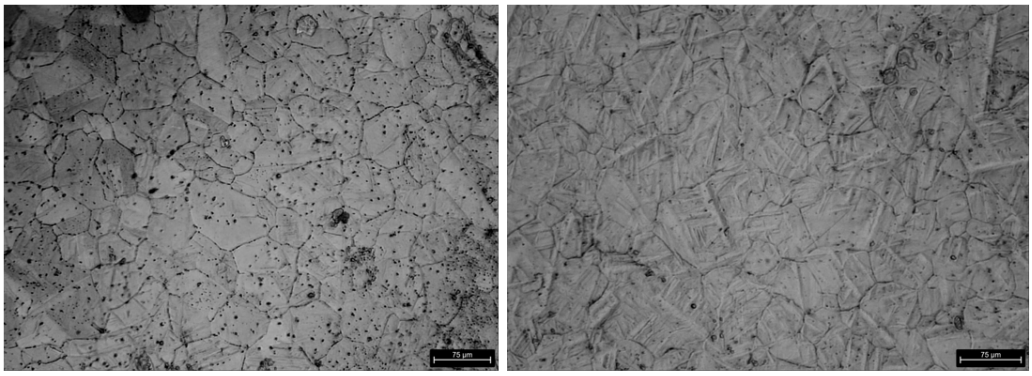

a) b)

Figure 4.11: OM micrographs depcting the grain boundaries of the condition (a) C7 and (b) S7.

The longest holding times have been observed to promote grain growth, which can subsequently result in a reduction in hardness [17, 58]. The formation of a coarser martensite is associated with an increase in the size of the austenitic grains. It was indeed observed that an increase in holding time by approximately 15 times resulted in an increase of the grain size by around 1.5 times. It is established that molybdenum can impede the rate of grain growth. Consequently, the increase in grain size when the holding time is significantly increased is not as significant as it would be if molybdenum

were not present. In accordance with the NADCA requirements, the grain size should be equal to or greater than grade 7 according to ASTM E112. This was observed in all conditions, thus rendering the application acceptable [7, 18, 22]. It can thus be concluded that the observed decrease in hardness was a consequence of the increase in grain size.

This analysis demonstrates that a reduction in holding time by 33 % (Appendix A) does not adversely affect the microstructure or mechanical properties of the material, thereby allowing its application. In this regard, triple tempering was conducted with the objective of achieving the shortest possible holding time. This was achieved by applying the C7 austenitisation condition for the centre, with a holding time of 20 minutes, and the S7 austenitisation condition for the surface, with a holding time of 425 minutes.

4.3 Quenched and Tempered Conditions

The nomenclature of the samples is in accordance with the conditions identified in Table 3.5 of Section 3.2. Figure 4.12 depicts the OM micrographs of the (a) central region of the tool (C7) and (b) surface of the tool (S7) following the application of the conventional tempering process, wherein the ΔT = 0 ºC. The SEM micrographs of the centre and surface of the tool can be found in 4.12 (c) and (d), respectively. From the observation of the micrographs, it can be concluded that there is a significant difference between the centre and the surface of the tool. The central region is distinguished by a finer martensitic structure and a more heavily dense carbide dispersion.

Figure 4.13 outlines the OM micrographs of the centre (C8) and surface (S8) of the tool when a ΔT = 10 ºC is applied during the tempering process. Figure 4.13 (c) and (d) represents the SEM images of the C8 and S8 regions, respectively. Once more, the microstructure is defined by a finer tempered martensitic matrix as well as a denser carbide dispersion when comparing the micrographs of the centre of the tool to those of the surface.

Figure 4.14 illustrates the SEM micrographs of the tool's centre (C9) and surface (S9) when a ΔT of 20 ºC was applied during austenitisation. Moreover, the corresponding OM images of C9 and S9 are presented in Figure 4.14 (c) and (d), respectively. As with the preceding samples, a discrepancy is evident between the microstructure of the centre and that of the surface.

Figure 4.15 depicts the quenched and tempered microstructure of AISI H11 Premium tool steel in the absence of a thermal gradient (S10). This results in the formation of a tempered martensitic matrix and a notable dispersion of carbides. This is illustrated in Figure 4.15 (a) and (b), which present the findings of OM and SEM analysis, respectively.

The microstructure of the quenched and tempered samples is characterised by a tempered martensitic matrix and a significant carbide dispersion, which was analysed through SEM coupled with EDS.

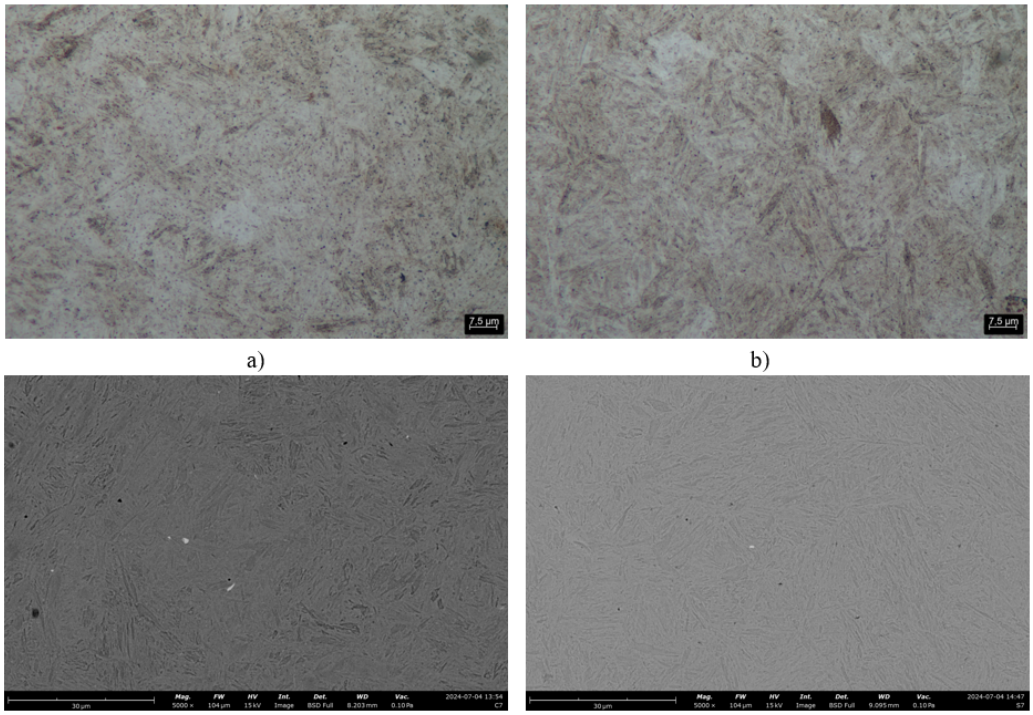

Figure 4.12: OM micrographs of quenched and tempered microstructure of the (a) centre (C7), with an austenitisation time of 20 minutes and tempering time of 120 minutes at 560 ºC and (b) surface (S7) of the tool, with an austenitisation time of 425 minutes and a tempering time of 210 minutes, also at 560 ºC, representing a martensitic matrix with a dispersion of primary and secondary carbides and SEM micrographs of (c) C7 and (d) S7.

It can be stated that the final microstructure resulting from triple tempering is significantly influenced by the initial, quenched microstructure. The preceding analysis demonstrated that the surface exhibited a coarser tempered martensitic structure than that observed in the centre, which remained consistent. If bainite is present in the quenched microstructure, it can be expected that this phase will transform as the tempering temperature is set above the start of the bainitic transformation, B_s, which is estimated to occur at approximately 400°C based on the available literature [44].

The microstructure of all sets of tempering conditions was found to be characterised by a tempered martensitic matrix and a dispersion of carbides, as previously described in the literature. It is anticipated that the quantity of retained austenite will diminish and approach zero following triple tempering. However, XRD analysis was not conducted, as the levels in question are challenging to discern when they fall below 5 %. Indeed, an examination of the CCT diagram indicates that the martensite finish temperature, M_f, can be identified at temperatures exceeding 100°C, suggesting that the entirety of the austenite would undergo transformation into martensite, at room temperature [18].

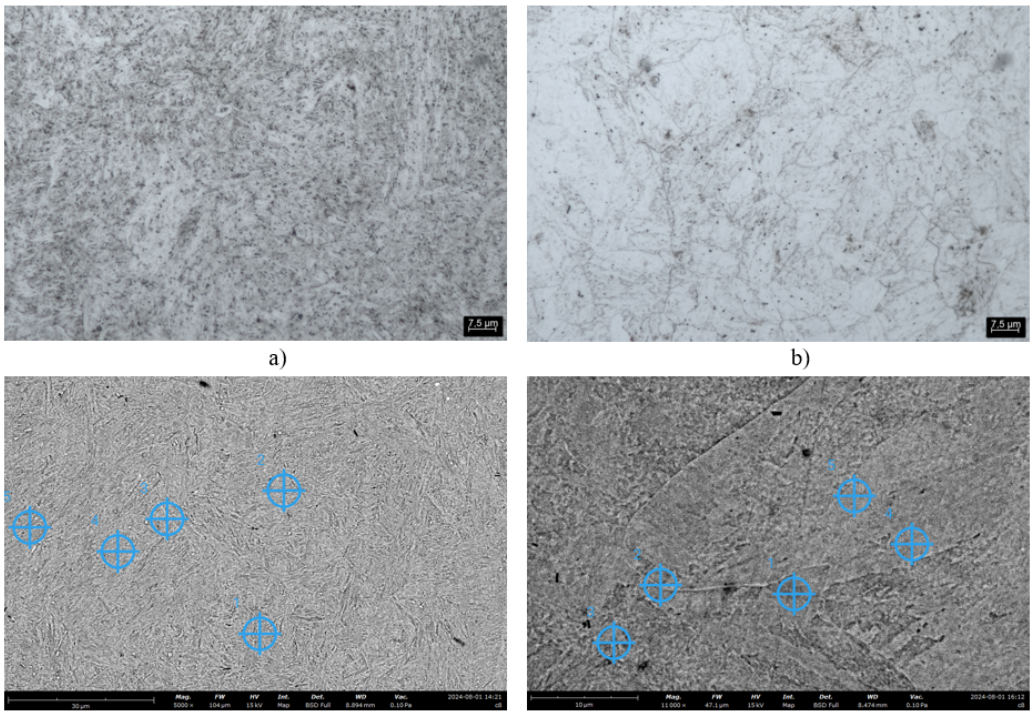

Figure 4.13: OM micrographs of quenched and tempered microstructure of the (a) centre (C8), with an austenitisation time of 20 minutes, tempering at 550 ºC for 40 minutes and at 560 ºC for 80 minutes and (b) surface (S8), with an austenitisation time of 425 minutes, tempering at 550 ºC for 128 minutes and at 560 ºC for 82 minutes, representing a martensitic matrix with a dispersion of primary and secondary carbides and SEM micrographs of (c) C8 and (d) S8.

As demonstrated in Section 3.2, for a heating rate of 12 ºC/min, a holding time of 30 min and a cooling rate of 50 ºC/s, the end of the martensitic transformation, M_f is approximately 80 ºC. However, given that these temperatures are situated in close proximity to room temperature and M_s and M_f are influenced by the chemical composition of austenite at the end of the austenitisation stage, it is not possible to assert with certainty that no austenite will be present to be transformed upon tempering, particularly given the detection of austenite through XRD. A discrepancy between the density of carbide dispersion in the conditions of the centre and that of the surface was qualitatively concluded through an analysis of the SEM micrographs of each sample. As previously described in Subsection 2.2.3, the nucleation of alloy carbides occurs at varying sites, including grain boundaries. An increase in grain size results in a reduction in the specific area of the grain boundary, which subsequently decreases the number of preferential sites for the nucleation of alloy carbides. This may be the reason behind the lower carbide dispersion observed for the surface conditions when compared to the centre [7, 8, 14, 22, 26]. Furthermore, a review of the literature indicates that for slower cooling rates at

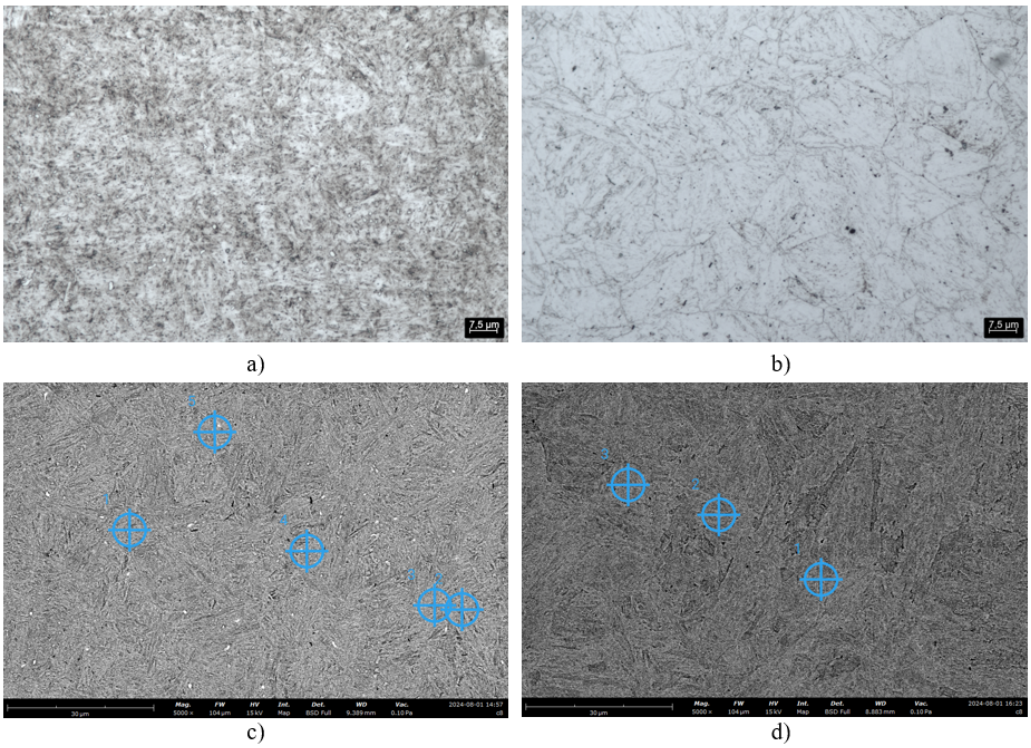

Figure 4.14: OM micrographs of quenched and tempered microstructure of the (a) centre (C9), with an austenitisation time of 20 minutes, tempering at 540 ºC for 40 minutes and at 560 ºC for 80 minutes and (b) surface (S9), with an austenitisation time of 425 minutes, tempering at 540 ºC for 127 minutes and at 560 ºC for 83 minutes, representing a martensitic matrix with a dispersion of primary and secondary carbides and SEM micrographs of (c) C9 and (d) S9.

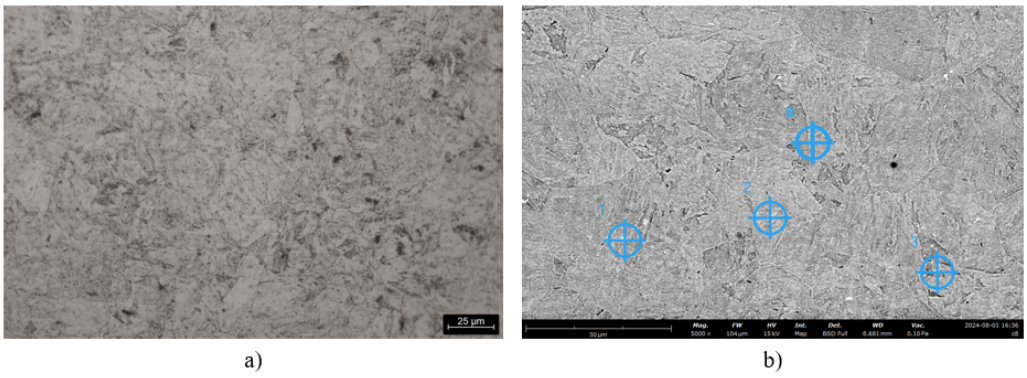

Figure 4.15: (a) OM micrograph of the condition corresponding to the absence of a thermal gradient (S10) and (b) its SEM micrograph, representing the tempered microstructure

quenching, such as those observed for air cooling, precipitates are formed preferentially at grain and lath boundaries [55].

Table 4.1 presents the results of carbide detection using SEM coupled with EDS. Significant discrepancies were identified between the carbides detected at the centre of the tool and those observed at the surface. Firstly, as previously stated, a denser carbide distribution was observed for the centre than for the surface. Additionally, it was qualitatively concluded that the carbides detected in the centre were finer than those detected for the surface, as depicted, previously, in Figure 4.12 to Figure 4.15. In general, the same types of carbides were detected in all sets of conditions at the centre, namely chromium-iron carbides, molybdenum-iron carbides and iron carbides. In the case of tempering at 560°C for the entire duration (S7), the presence of iron, chromium-iron and vanadium-iron carbides was confirmed. Upon conducting a step at a temperature 10 ºC below the set temperature (S8), the presence of iron carbides was confirmed. Conversely, when a step was performed at 20 ºC below the set temperature (S9), both iron and iron-molybdenum carbides were identified. The condition that exhibited no thermal gradients (S10) demonstrated the presence of molybdenum-iron and chromium-iron carbides. The morphology of these carbides was discernible through SEM, and is also presented in Table 4.1.

Table 4.1: SEM detected carbides' type and morphology of the quenched and tempered samples.

ID	Detetcted Carbides' Type	Morphology
C7	Cr - Fe	Large globular carbides
		Small globular carbides
C8	Mo - Fe	Large elongated carbides
C9		Large globular carbides
	Fe	Globular carbides
S7	Fe	Globular carbides
	V - Fe	Small globular carbides
	Cr - Fe	Small globular carbides
S8	Fe	Globular carbides
S9	Fe	Globular carbides
	Mo - Fe	Globular carbides
S10	Mo - Fe	Elongated carbides
		Large globular carbides
	Cr - Fe	Small globular carbides

Figure 4.16 illustrates the findings of the carbide identification conducted using SEM coupled with EDS on condition C8. The analysis enabled the identification of carbides comprising iron and molybdenum, as well as chromium and iron. Furthermore, it can be observed that a fine martensitic structure is present, accompanied by a dispersion of carbides.

Following the tempering process, the formation of carbides of the MC, M_3C, M_7C_3 and $M_{23}C_6$ types is anticipated, corresponding to vanadium-iron, iron and chromium-iron carbides [7, 22, 25, 59,

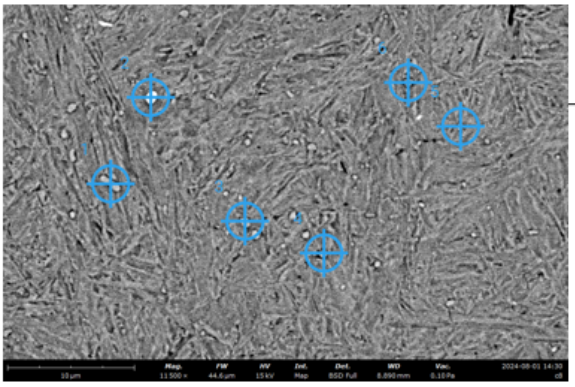

Spot	Elements Weight Concentration (%)					Possible Carbide Type
	C	V	Cr	Fe	Mo	
1	5.4	2.1	20.2	64.3	6.4	$M_{23}C_6$
2	7.3	1.8	4.5	50	35.2	M_2C
3	7.0	2.6	24.9	56.3	7.6	M_7C_3
4	6.8	3.3	24.4	60.3	2.9	M_7C_3
5	5.6	1.7	14.8	73.6	4.3	M_7C_3 or $M_{23}C_6$
6	7.8	4.8	27.4	54.4	3.9	M_7C_3

Figure 4.16: Identification of the carbides present in the sample related to condition C8, with the application of SEM/EDS.

60]. Indeed, the samples corresponding to the centre presented evidence of the presence of carbides comprising iron, molybdenum and chromium. The absence of vanadium carbides may be attributed to insufficient nucleation time, or a lack of sufficient magnification to discern their presence [55]. The presence of molybdenum-iron carbides may be attributed to their non-dissolution during austenitisation, as evidenced by their presence in the quenched microstructure [54]. In addition to the reduced density of the carbide dispersion, the surface conditions exhibit a markedly diminished range of carbide types when a ΔT of 10 and 20 ºC (S8 and S9, respectively) is applied. As outlined in Subsection 2.2.3, the nucleation of alloy carbides is only observed at temperatures exceeding 550°C. This could account for the prevalence of iron carbides, as the samples in question undergo tempering at 550°C and 540°C for approximately two-thirds of the total tempering time. Additionally, chromium may not have the sufficient time or adequate temperature to migrate from the matrix to the M_3C carbide and form M_7C_3. The precipitation of molybdenum and vanadium carbides occurs independently of M_3C, which explains why they are observed with greater frequency than chromium-rich carbides when M_3C is detected [55]. A review of the literature reveals that, in the case of low weight percentages of silicon, as observed in AISI H11 Premium tool steel, the majority of the alloying elements are contingent upon the dissolution of cementite particles in order to form their preferred alloy carbides [57]. The presence of stabilised cementite particles will result in a shift in the precipitation of fine alloy carbides, with the process occurring at higher temperatures or over longer tempering times. Furthermore, the presence of iron-molybdenum carbides may be attributed to their non-dissolution during austenitisation, as observed in the centre conditions. However, the conventional tempering parameters yielded the presence of chromium-iron, iron, and vanadium-iron carbides. The aforementioned carbide was not observed in any other sample, which may be attributed to the longest tempering time at 560°C of this sample when compared to the remaining samples. Ultimately, the condition that

resolved the discrepancy between the surface and centre presented molybdenum-iron and chromium-iron carbides, indicating that all iron carbides, potentially cementite, underwent transformation into complex carbides. It was ultimately determined that the vast majority of carbides exhibited a globular morphology. As demonstrated by Mayer *et al.*, the precipitation of carbides with a spherical morphology is dependent on the cooling rate following quenching [55]. It is anticipated that the precipitation sequence will conclude with $M_{23}C_6$However, the presence of vanadium has been observed to stabilise M_7C_3, which could explain the more pronounced observation of what we have deduced to be M_7C_3 carbides in comparison to $M_{23}C_6$ [25].

Figure 4.17 illustrates the impact of the tempering parameters, namely temperature and time, on the ultimate hardness of the AISI H11 Premium tool steel. It is noteworthy that the conditions pertaining to the central region (C7 to C9) exhibited a hardness of 53 HRC $\pm$ 1 HRC at the outset, whereas the surface conditions (S7 to S9) commenced at a hardness of 46 HRC $\pm$ 1 HRC. In contrast, S10 demonstrated a hardness of 51 HRC $\pm$ 1 HRC following quenching. Following the application of the conventional triple tempering parameters, the central region exhibited a hardness of 50 HRC $\pm$ 2 HRC, while the surface displayed a hardness of 45 HRC $\pm$ 1 HRC. When a step is performed 10 ºC below the desired tempering time, and consequently the permanence for a third of the tempering time at 550 ºC, the resulting hardness is 54 HRC $\pm$ 1 for the centre and 42 HRC $\pm$ 3 HRC for the surface of the tool. A step performed 20 ºC below the desired tempering time, and consequently the permanence for a third of the tempering time at 540 ºC, resulted in a hardness of 50 HRC $\pm$ 1 HRC at the centre of the tool and 44 HRC $\pm$ 1 HRC at the surface. Ultimately, condition S10 exhibited a decline in hardness, reaching a value of 50 HRC $\pm$ 1 HRC.

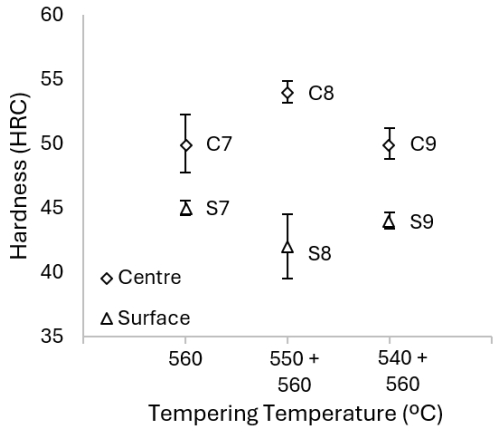

Condition	Holding Time (Austenitisation) (min)	Tempering Time (min)	
		$t_{\Delta T}$	t
C7		0	120
C8	20	40	80
C9		40	80
S7		0	210
S8	425	128	82
S9		127	83

Figure 4.17: Hardness (HRC) of the quenched and tempered samples and respective tempering parameters.

Subsequent to the tempering procedure, the material is anticipated to demonstrate hardness values

within the range of 42 to 52 HRC. The precise targeted value is contingent upon the intended final application of the material, as well as the specific characteristics of the material itself. In the process of triple tempering at 560°C, the heat treatment is conducted at a temperature that exceeds the secondary hardening peak. This approach prevents an increase in hardness and a potential subsequent reduction in the toughness of the AISI H11 Premium steel, which is dependent on the hardness values of the centre of the tool, 50 HRC $\pm$ 2 HRC and the surface, 45 HRC $\pm$ 1 HRC. These values are in accordance with those observed in the literature [18, 57, 59]. Nevertheless, it has been demonstrated that subjecting the material to a brief period of the tempering time at temperatures within the secondary hardening range (500 - 550 ºC) can have a detrimental effect on its properties. Indeed, when triple tempering was performed at 550 ºC (40 minutes for the centre and 128 minutes for the surface) and 560 ºC (80 minutes for the centre and 83 minutes for the surface), an increase in the hardness of the material in the centre of the tool was observed, reaching values of 54 HRC $\pm$ 1 HRC, which is corroborated by the presence of a dense dispersion of complex carbides in the tempered martensitic matrix. The same phenomenon was not observed at the surface, likely due to the presence of fewer nucleation sites, as previously discussed, which reduced the secondary hardening effect [2, 5, 14, 22, 24, 25]. Additionally, the surface exhibited a lower hardness than the centre, after quenching, with a value of 46 HRC $\pm$ 1 HRC, which subsequently resulted in a decrease to 42 HRC $\pm$ 3 HRC. Ultimately, triple tempering at 540 (40 minutes for the centre and 127 minutes for the surface) and 560°C (80 minutes for the centre and 83 minutes for the surface) resulted in a reduction in material hardness, both in the centre (50 HRC $\pm$ 1 HRC) and on the surface of the tool (44 HRC $\pm$ 1 HRC).

Table 4.2 presents the variation in CVN against tempering temperature for each heat treatment sequence. As the time spent at the highest temperature (560°C) is increased, the absorbed energy rises at the surface. Furthermore, it is evident that there is a discrepancy between the absorbed energy observed for the conditions pertaining to the centre and those of the surface. The centre exhibited values between 9 and 11 J, while the surface demonstrated values between 15 and 18 J. These findings indicate that the absorbed energy of the conditions was not significantly different in either case. The lower absorbed energy observed for the centre can be attributed to two factors. Firstly, the centre exhibits a higher hardness value after quenching. Secondly, the precipitation of carbides was observed to be higher for this set of conditions. A review of the literature revealed comparable values of absorbed energy for analogous tempering conditions [18, 30, 61, 62]. Furthermore, in the absence of thermal gradients, an absorbed energy of 8 J $\pm$ 1 J is anticipated, representing the lowest value observed across all studied conditions. It is crucial to acknowledge that these values are associated with the rolling perpendicular direction, which is the most susceptible to damage. Consequently, the other directions will demonstrate higher values of absorbed energy.

Table 4.2: The absorbed energy, in Joules, for the various tested conditions.

Condition ID	C7	C8	C9	S7	S8	S9	S10
Absorbed Energy (J)	11 ± 1	10 ± 1	9 ± 3	18 ± 0	15 ± 0	15 ± 1	8 ± 1

Figure 4.18 illustrates the variation in hardness and toughness with respect to the tempering conditions. The values are plotted in ascending order of tempering time at 560°C, for the centre and surface, respectively. As anticipated, the hardness and toughness curves exhibit a reciprocal relationship. When the hardness curve declines, the toughness curve demonstrates an increase [30]. The optimal heat treatment strategy is a combination of superior hardness and high toughness, which allows for the maintenance of a high degree of dimensional accuracy while preventing fracture failure. A preliminary investigation suggests that the optimal combination of high hardness and high toughness is achieved when tempering starts at 20 ºC below the set temperature (540+ 560 ºC). Nevertheless, additional mechanical assessments, such as tensile tests, are essential to ascertain the ultimate tensile strength, yield strength, and, most crucially, the ductility of the material. This ensures the material's formability and the prevention of failure due to defects such as cracks.

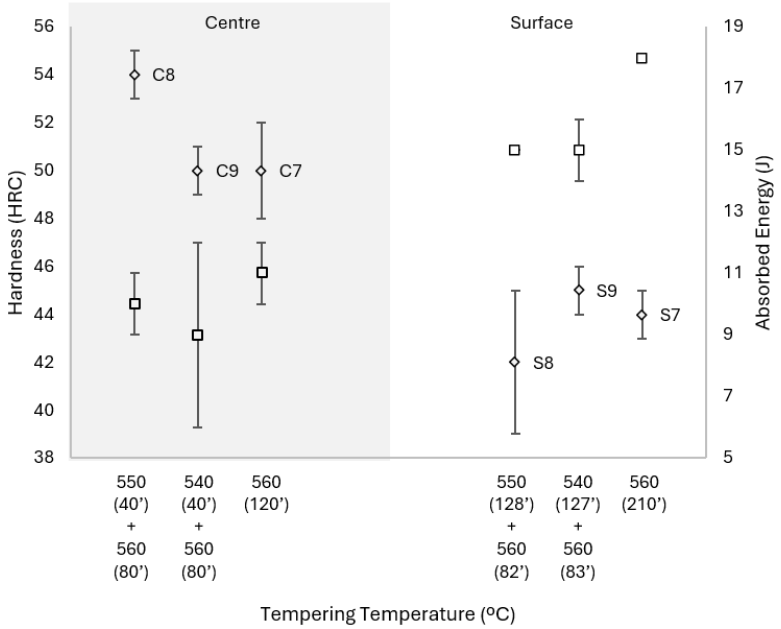

Figure 4.18: Hardness (HRC) and absorbed energy (J) of the quenched and tempered samples and respective tempering parameters.

In order to gain a deeper understanding of the relationship between hardness and absorbed energy, a linear regression analysis was conducted. Indeed, this analysis, presented in Figure 4.19, indicates

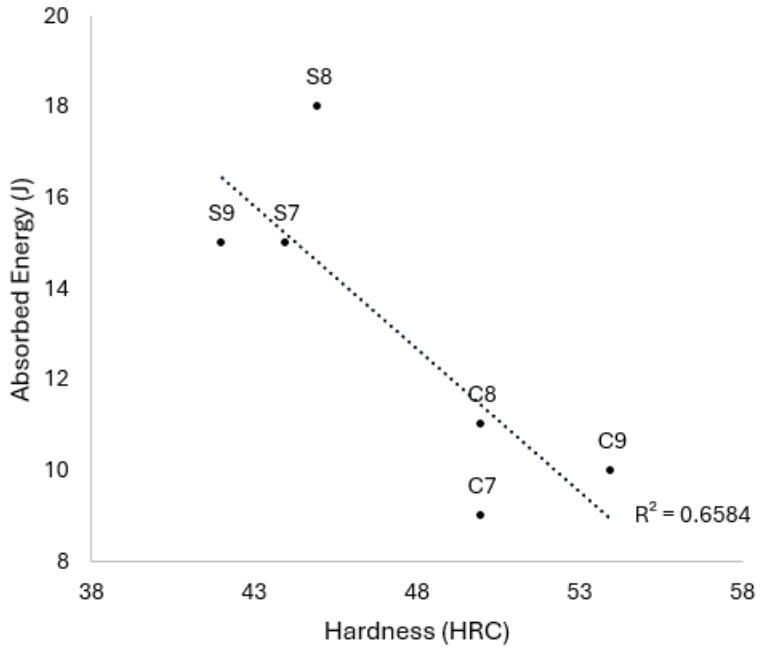

Figure 4.19: Linear regression correlating the hardness and the absorbed energy of the quenched and tempered conditions.

that there is a strong negative linear relationship between absorbed energy and hardness (r = -0.811). Indeed, approximately 65 % (R^2 = 0.6584) of the variation in absorbed energy may be explained by the variation in the hardness of the AISI H11 Premium steel.

Chapter 5

Conclusions and Future Work

5.1 Conclusions

The principal objective of this study was to enhance the heat treatment of AISI H11 Premium steel by reducing holding times through the utilisation of a ΔT, with the ultimate goal of reducing heat treatment costs. The specifics of the time reduction calculation are outlined in the Appendix A [63]. The microstructure, hardness and absorbed energy analyses yielded several noteworthy findings that correlated with the holding time and temperature of both quenching and triple tempering. The mechanical behaviour was evaluated and correlated with the findings from microstructural characterisation, and the following conclusions were drawn:

- Starting the heat treatment 20 ºC below the austenitising temperature during the quenching step revealed that a 33 % reduction in holding time for the central region of the tool was feasible while ensuring sufficient time for austenitisation. This resulted in a martensitic matrix with a retained austenite volume of 5 % or less and a minor dispersion of undissolved molybdenum and iron carbides.
- Following quenching, the centre exhibited hardness values between 53 and 54 HRC. In contrast, the surface exhibited hardness values between 46 and 47 HRC. The values indicated demonstrate that the material in question has attained the requisite hardness following quenching. Furthermore, it was established that the disparity in hardness between the centre and surface of the tool was a consequence of grain growth induced by the extended holding times.
- The application of triple tempering results in the formation of a tempered martensitic matrix and the dispersion of carbides, irrespective of the specific tempering cycle employed. However, the

centre of the tool exhibits a greater density of carbide dispersion in comparison to the surface, due to the presence of a greater number of nucleation sites, which facilitate carbide formation.

- Cycle optimization seam to be possible and advisable, as hardness and absorbed energy are set at acceptable values, ranging from 42 to 54 HRC and 10 to 18 J, respectively, in all studied conditions. When starting both quenching and tempering at 20 ºC under both set temperatures, we obtain a tempered martensitic matrix with a significant dispersion of Fe, Mo and Cr rich carbides, a hardness of 50 $\pm$ 1 HRC and an absorbed energy of 9 $\pm$ 3 J, properties related to the centre of the tool and a hardness of 44 $\pm$ 1 HRC and an absorbed energy of 15 $\pm$ 1 J for the surface of the tool.

5.2 Future Work

Upon the conclusion of this study, there are approaches for further testing and experimentation that could enhance and complete the scope of this research.

- Conduct tensile tests on the heat treated conditions to access the ultimate tensile strength, yield strength and ductility with a view to better correlating these characteristics with those of the microstructure, as well as with hardness and absorbed energy .
- Study the microstructure and mechanical properties after each tempering stage, to ascertain the influence and evolution of each stage on the performance of the AISI H11 premium steel, including the impact of performing three tempering stages instead of two.
- Explore the potential benefits of starting the heat treatment more than 20 ºC under the desired temperature, during quenching and tempering.
- A TEM analysis should be performed in order to identify the composition and crystalline structure of the carbide, and to correlate these findings with the mechanical properties.

References

[1] Uddeholm AB. Die Casting, 2018.

[2] George A. Krauss, George A. Roberts, and Richard L. Kennedy. 13. Hot-Work Tool Steels. In *Tool steels*. ASM International, Materials Park, Ohio, 5 edition, 1998.

[3] Dean Kouprianoff and Willie Du Preez. Reducing time and cost of the heat treatment post-processing of additively manufactured Ti6Al4V. *Materials Today Communications*, 35, June 2023.

[4] Noor Zaman Khan, Sheikh Shahid Ul Islam, Mohammad Mohsin Khan, and Arshad Noor Siddiquee. Steel heat treatment: Equipment and process design. In *Reference Module in Materials Science and Materials Engineering*. Elsevier, 2024.

[5] J. Dossett and G. E. Totten. 23. Heat Treating of Hot-Work Tool Steels. In *ASM Handbook, Volume 4D Heat Treating of Irons and Steels*. ASM International, Materials Park, Ohio, 10th edition edition, 2014.

[6] Erik Oberg, Franklin D. Jones, Holbrook Lynedon Horton, Henry H. Ryffel, Christopher J. McCauley, and Laura Brengelman. *Machinery's handbook*. Industrial Press, Inc, South Norwalk, Connecticut, 31st edition, 2020.

[7] R. A. Mesquita, C. A. Barbosa, and A. R. Machado. 2.9 Heat Treatment of Tool Steels. In *Comprehensive Materials Finishing*, pages 214–245. Elsevier, Oxford, 2017.

[8] ASM Internation Handbook Committee, editor. *ASM handbook. 4: Heat treating*. ASM International, Materials Park, Ohio, 9. print edition, 1991.

[9] George A. Krauss, George A. Roberts, and Richard L. Kennedy. 2. Classification and Selection of Tool Steels. In *Tool steels*. ASM International, Materials Park, Ohio, 5. ed edition, 1998.

[10] International Organization for Standardization. Tool Steels (ISO 4957: 2018), 2018.

[11] Ramada Aços. 2343, May 2022.

[12] Ramada Aços. Uddeholm Vidar Superior, May 2022.

[13] R. A. Mesquita and H.-J. Kestenbach. Complete model for effects of silicon in 5%Cr hot work tool steels. *International Heat Treatment and Surface Engineering*, 4(4):145–151, 2010.

[14] B. Podgornik, B. Žužek, F. Kafexhiu, and V. Leskovšek. Effect of Si Content on Wear Performance of Hot Work Tool Steel. *Tribology Letters*, 63(1):5, 2016.

[15] D. Delagnes, P. Lamesle, M.H. Mathon, N. Mebarki, and C. Levaillant. Influence of silicon content on the precipitation of secondary carbides and fatigue properties of a 5%Cr tempered martensitic steel. *Materials Science and Engineering: A*, 394(1-2):435–444, 2005.

[16] Rafael Agnelli Mesquita and Hans-Jürgen Kestenbach. Influence of silicon on secondary hardening of 5wt% Cr steels. *Materials Science and Engineering: A*, 556:970–973, 2012.

[17] Karl-Erik Thelning. 5 - Heat treatment—general. In *Steel and its Heat Treatment*, pages 177–260. Elsevier, 1975.

[18] Uddeholm AB. Uddeholm Vidar Superior, 2013.

[19] Myrna Mochtar and Wahyuaji Putra. Effect of Austenitizing Temperature and Holding Time on Microstructure, Hardness, and Retained Austenite Amount of HSLA Steel as Automotive Components Material. *Joint Journal of Novel Carbon Resource Sciences & Green Asia Strategy*, 11:462–469, March 2024.

[20] William E. Bryson. *Heat Treatment: Master Control Manual*. Hanser, München, 2015.

[21] NADCA DIE MATERIALS COMMITTEE. *Special Quality Die Steel & Heat Treatment Acceptance Criteria for Die Casting Dies*. North American Die Cating Association, Illinois, 2018.

[22] Harshad Bhadeshia and Robert Honeycombe. 9. Tempering of Martensite. In *Steels: Microstructure and Properties*, pages 237–270. Elsevier, 2017.

[23] Vojteh Leskovšek, Borivoj Šuštaršič, and Gorazd Jutriša. The influence of austenitizing and tempering temperature on the hardness and fracture toughness of hot-worked H11 tool steel. *Journal of Materials Processing Technology*, 178(1-3):328–334, 2006.

[24] B. Podgornik, V. Leskovšek, F. Tehovnik, and J. Burja. Vacuum heat treatment optimization for improved load carrying capacity and wear properties of surface engineered hot work tool steel. *Surface and Coatings Technology*, 261:253–261, 2015.

[25] N. Mebarki, D. Delagnes, P. Lamesle, F. Delmas, and C. Levaillant. Relationship between microstructure and mechanical properties of a 5% Cr tempered martensitic tool steel. *Materials Science and Engineering: A*, 387-389:171–175, 2004.

[26] Tushar R. Dandekar and Rajesh K. Khatirkar. Structural and wear assessment of H11 die steel as a function of tempering temperature. *Materials Today: Proceedings*, 2023.

[27] Christoph Lerchbacher, Silvia Zinner, and Harald Leitner. Direct or indirect: Influence of type of retained austenite decomposition during tempering on the toughness of a hot-work tool steel. *Materials Science and Engineering: A*, 564:163–168, 2013.

[28] ASM Internation Handbook Committee. Process and Quality Control Considerations. In *ASM Handbook: Heat Treating*, volume 4, pages 529–541. ASM International, 1991.

[29] M. Korecki, J. Olejnik, P. Kula, and E. Wołowiec. Meeting standards for die heat treatment. *International Heat Treatment and Surface Engineering*, 8(4):183–187, December 2014.

[30] Sayyad Zahid Qamar, Majid Al-Maharbi, and Tasneem Pervez. Thermal material enhancement of metalformimg die steel. In *Reference Module in Materials Science and Materials Engineering*. Elsevier, 2024.

[31] Rok Markežič, Nikolaj Mole, Iztok Naglič, and Roman Šturm. Time and temperature dependent softening of H11 hot-work tool steel and definition of an anisothermal tempering kinetic model. *Materials Today Communications*, 22, 2020.

[32] M.K. Banerjee. 2.8 Heat Treatment of Commercial Steels for Engineering Applications. In *Comprehensive Materials Finishing*, pages 180–213. Elsevier, 2017.

[33] James A. Szumera. Heat Treatment of Tool Steels. In *The Tool Steel Guide*. Industrial Press, New York, NY, 1st ed edition, 2003.

[34] G. F. Vander Voort. *ASM handbook. 9: Metallography and microstructures*. ASM International, Materials Park, Ohio, 1. print edition, 2004.

[35] G. F. Vander Voort. 44. Metallographic Techniques for Tool Steels. In *ASM handbook. 9: Metallography and microstructures*. ASM International, Materials Park, Ohio, 1. print edition, 2004.

[36] S. S. M. Tavares, S. R. Mello, A. M. Gomes, J. M. Neto, M. R. Da Silva, and J. M. Pardal. X-ray diffraction and magnetic characterization of the retained austenite in a chromium alloyed high carbon steel. *Journal of Materials Science*, 41(15):4732–4736, August 2006.

[37] Dennis W. Hetzner. X-Ray Determination of Retained Austenite in Steel Using ASTM E975. *Microscopy and Microanalysis*, 9(S02):710–711, August 2003.

[38] M. Pérez, C. Rodríguez, and F.J. Belzunce. The Use of Cryogenic Thermal Treatments to Increase the Fracture Toughness of a Hot Work Tool Steel Used to Make Forging Dies. *Procedia Materials Science*, 3:604–609, 2014.

[39] Bernard Dennis Cullity. *Elements of X-ray diffraction*. Addison-Wesley series in metallurgy and materials. Addison-Wesley publ, Reading (Mass.) Menlo Park (Calif.) London [etc.], second ed edition, 1978.

[40] American Society for Testing and Materials. Standard Test Methods for Determining Average Grain Size (ASTM E112), 2021.

[41] C. Kim, V. Biss, and W. F. Hosford. A New Procedure for Determining Volume Fraction of Primary Carbides in High-Speed and Related Tool Steels. *Metallurgical Transactions A*, 13(2):185–191, February 1982.

[42] H. Goldenstein and J. A. Cifuentes. Overall kinetics and morphology of the products of austenite decomposition in a Fe-0.46 Pct C-5.2 Pct Cr alloy transformed isothermally above the bay. *Metallurgical and Materials Transactions A*, 37(6):1747–1755, June 2006.

[43] Instituto Português da Qualidade. Metallic Materials Charpy Pendulum Impact Test Part 1: Test Method (ISO 148-1 2009), 2015.

[44] Michal Krbaťa, Maroš Eckert, Róbert Cíger, and Marcel Kohutiar. Physical modeling of CCT diagram of tool steel 1.2343. *Procedia Structural Integrity*, 43:270–275, 2023.

[45] Jie Wei, Yangtao Zhou, Junhua Dong, Xiaoyan He, and Wei Ke. Effect of cementite spheroidization on improving corrosion resistance of pearlitic steel under simulated bottom plate environment of cargo oil tank. *Materialia*, 6:100316, June 2019.

[46] Grzegorz Łukaszewicz, Marcin Szczygieł, Monika Węsierska-Hinca, Krzysztof Chmielarz, Edyta Wierzbicka, and Krzysztof Wasiak. Interrupted quenching and bainitising below Ms temperature of EN X37CrMoV5-1 hot-work tool steel: Bainitic transformation kinetics, microstructure and mechanical properties. *Materials Science and Engineering: A*, 869:144740, March 2023.

[47] George Krauss. *Steels: processing, structure and performance*. ASM International, Materials Park, Ohio, second edition, 2015.

[48] T. Maki. 2. Morphology and substructure of martensite in steels. In *Phase Transformations in Steels*, pages 34–58. Elsevier, 2012.

[49] Minoru Umemoto, Eizoh Yoshitake, and Imao Tamura. The morphology of martensite in Fe-C, Fe-Ni-C and Fe-Cr-C alloys. *Journal of Materials Science*, 18(10):2893–2904, October 1983.

[50] Wilson Handoko, Farshid Pahlevani, and Veena Sahajwalla. Effect of austenitisation temperature on corrosion resistance properties of dual-phase high-carbon steel. *Journal of Materials Science*, 54(21):13775–13786, November 2019.

[51] M L Fares, M Athmani, Y Khelfaoui, and A Khettache. An investigation into the effects of conventional heat treatments on mechanical characteristics of new hot working tool steel. *IOP Conference Series: Materials Science and Engineering*, 28:012042, February 2012.

[52] M.J. Peet. Bainitic steels and alloys for power plants. In *Structural Alloys for Power Plants*, pages 153–187. Elsevier, 2014.

[53] László Tóth. The possibilities of the retained austenite reduction on tool steels. *European Journal of Materials Science and Engineering*, 6(2):99–105, June 2021.

[54] Minwoo Kang, Gyujin Park, Jae-Gil Jung, Byung-Hoon Kim, and Young-Kook Lee. The effects of annealing temperature and cooling rate on carbide precipitation behavior in H13 hot-work tool steel. *Journal of Alloys and Compounds*, 627:359–366, April 2015.

[55] Mayer, S. Changes in Tempering and its Effect on Precipitation Behaviour in a Hot-work Tool Steel. *Steel Research International*, 80, No. 1 89-95, January 2009.

[56] Jon L. Dossett and George E. Totten. *ASM handbook, Volume 04D - Heat Treating of Irons and Steels*. ASM International, Materials Park, Ohio, 10th edition, 2014.

[57] R. A. Mesquita, C. A. Barbosa, E. V. Morales, and H.-J. Kestenbach. Effect of Silicon on Carbide Precipitation after Tempering of H11 Hot Work Steels. *Metallurgical and Materials Transactions A*, 42(2):461–472, February 2011.

[58] Karl-Erik Thelning. 6 - Heat treatment—special. In *Steel and its Heat Treatment*, pages 177–260. Elsevier, 1975.

[59] B. Podgornik, G. Puš, B. Žužek, V. Leskovšek, and M. Godec. Heat Treatment Optimization and Properties Correlation for H11-Type Hot-Work Tool Steel. *Metallurgical and Materials Transactions A*, 49(2):455–462, February 2018.

[60] Sylvain Dépinoy, C. Toffolon.Madclet, A. F. Gourgues, Ernst Kozeschnik, Bernard Marini, and François Roch. Evolution of microstructure during tempering and its influence on the mechanical behavior of 2.25Cr-1Mo bainitic steel. In *PTM 2015*, June 2015.

[61] Sanjeev Katoch, Vishal Singh, and Rakesh Sehgal. Mechanical Properties and Microstructure Evaluation of Differently Cryogenically Treated AISI-H11 Steel. *International Journal of Steel Structures*, 19(5):1381–1392, October 2019.

[62] A. Pastor, P. Valles, W. More, and S.F. Medina. Toughness improvement of steel X38CrMoV5-1 via alternative manufacturing process and prevention of catastrophic failure in safety parts. *Engineering Failure Analysis*, 82:791–801, December 2017.

[63] ASM International. Calculation of Heat Treating Costs. In *ASM handbook 04B*. ASM International, Materials Park, Ohio, 10th edition, 1990.

Appendix A

Calculating of Heat Treating Impact

To calculate the reduction in time resulting from the application of a ΔT, the following assumptions have been taken into account, as shown in Table A.1. The values presented are derived from the experimental procedure, specifically the heat treatment cycles performed on AISI H11 Premium steel, as outlined in Chapter 3.

Table A.1: Conditions and parameters used to calculate time reduction.

	Conditions and parameters
1	Austenitisation heating rate (core) = 2 ºC/min
2	Austenitisation heating rate (surface) = 12 ºC/min
3	Holding time (core) = 30 minutes
4	Tempering heating rate (core) = 2 ºC/min
5	Tempering heating rate (surface) = 3 ºC/min
6	Tempering holding time (core) = 120 minutes
7	The holding time for the surface is dependent on the heating rate of the core. This means that the surface will remain at the austenitising tempering and at the tempering temperatures for a longer time than the core
8	The calculation is based on Δt, which is the time that the component is kept at a temperature between T - ΔT and T

Appendix B

XRD Analysis

This appendix presents the processed data of the analysis of the XRD patterns, with the objective of determining the peaks of austenite and martensite in the samples that have been subjected to quenching, as well as the peaks of the carbides extracted from the as-received sample.

B.1 Retained Austenite

This section comprises the processed XRD patterns and the identification of austenite and martensite peaks for all samples that have undergone quenching. Figure B.1 to Figure B.3 refer to the conditions related to the centre. On the other hand, Figure B.4 to Figure B.6 represent the surface conditions. Finally, Figure B.7 represents the XRD pattern obtained for the conditions that could be attained when the centre and the surface of the component do not differ in terms of heating and cooling rates.

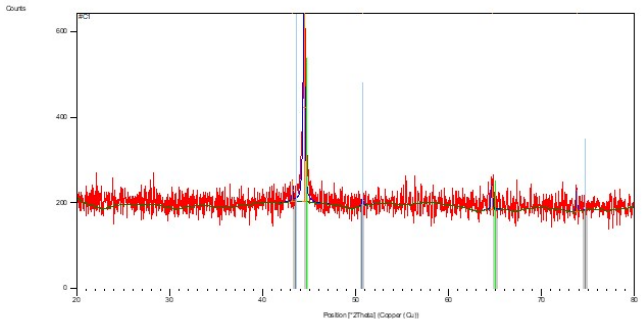

Figure B.1: XRD Pattern for the condition C1.

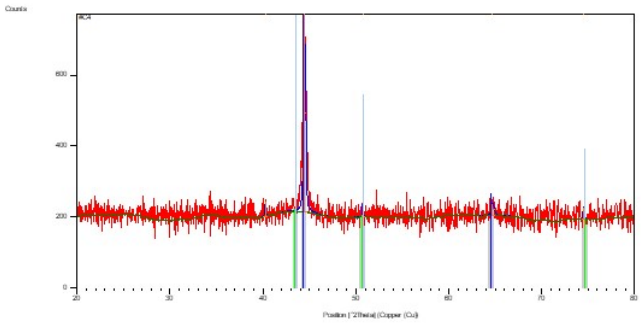

Figure B.2: XRD Pattern for the condition C4.

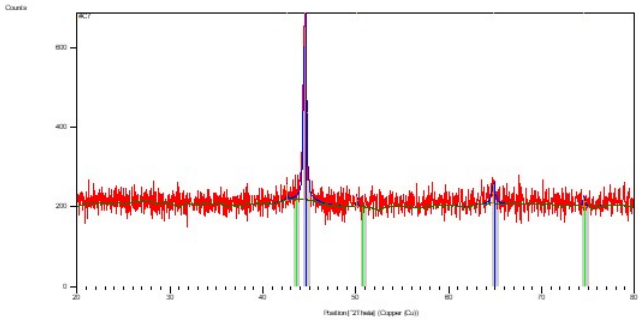

Figure B.3: XRD Pattern for the condition C7.

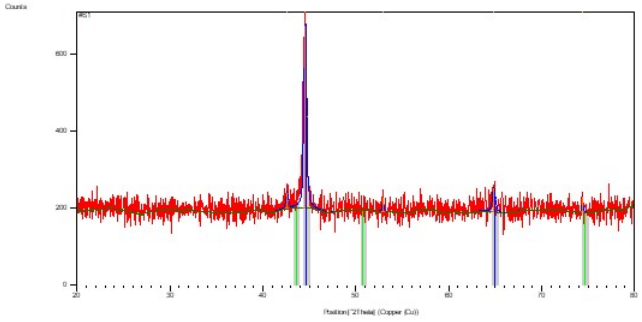

Figure B.4: XRD Pattern for the condition S1.

B.2 Extracted Carbides

This section comprises the processed XRD patterns and the identification of carbide peaks of the annealed sample. Figure B.8 refers to the samples dissolved in the Berzlius reagent. On the other

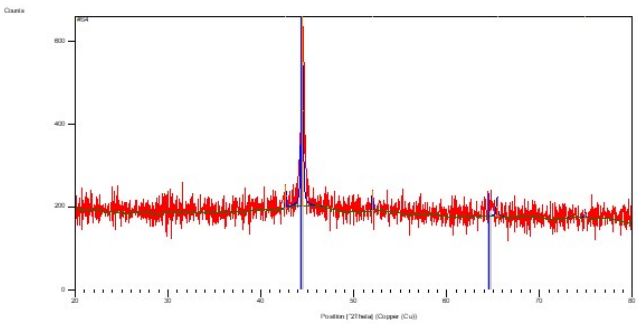

Figure B.5: XRD Pattern for the condition S4.

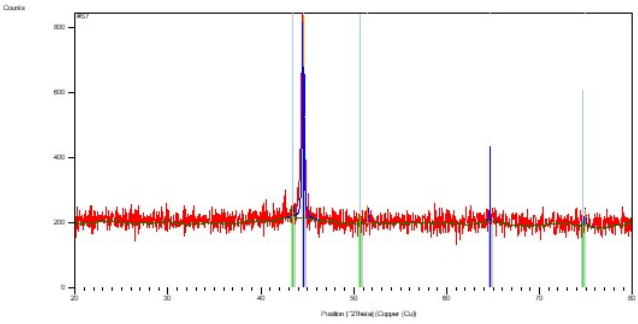

Figure B.6: XRD Pattern for the condition S7.

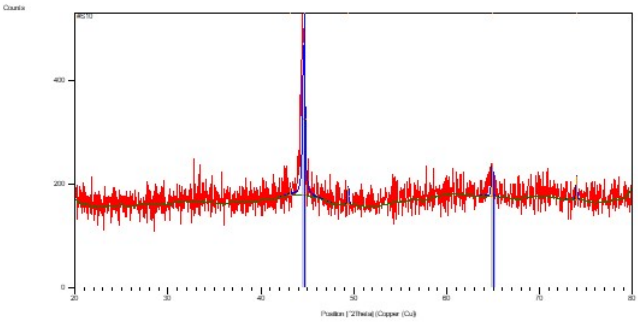

Figure B.7: XRD Pattern for the condition S10.

hand, Figure B.9 the samples dissolved in 10 % Nital.

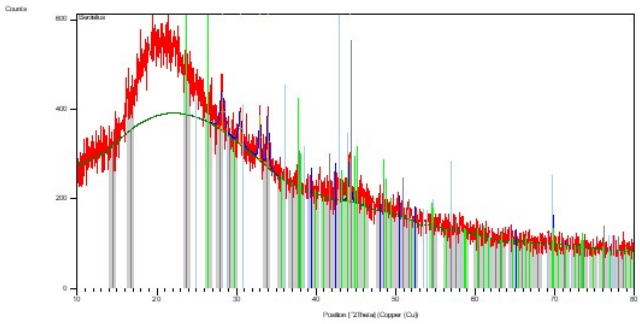

Figure B.8: XRD Pattern for the the extracted carbides from the Berzelius reagent.

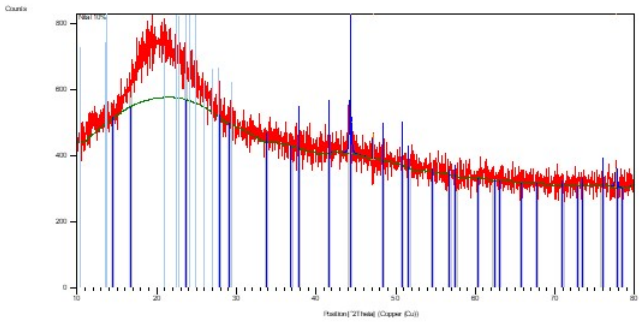

Figure B.9: XRD Pattern for the the extracted carbides from the Berzelius reagent.